Article

Joint Multi-Scenario-Based Earthquake and Tsunami Hazard Assessment for Alexandria, Egypt

Hazem Badreldin [1,2,*]**, Hany M. Hassan** [1,2]**, Fabio Romanelli** [3]**, Mahmoud El-Hadidy** [1] **and Mohamed N. ElGabry** [1]

1   National Research Institute of Astronomy and Geophysics, Helwan, Cairo 11421, Egypt; helsayed@ogs.it (H.M.H.); elhadidy.ms@nriag.sci.eg (M.E.-H.); elgabry@nriag.sci.eg (M.N.E.)
2   National Institute of Oceanography and Applied Geophysics-OGS, 34010 Trieste, Italy
3   Department of Mathematics, Informatics and Geosciences, University of Trieste, 34128 Trieste, Italy; romanel@units.it
*   Correspondence: hbadreldin@ogs.it or hazem.youssef@nriag.sci.eg

Abstract: The available historical documents for the city of Alexandria indicate that it was damaged to varying degrees by several (historical and instrumentally recorded) earthquakes and by highly destructive tsunamis reported at some places along the Mediterranean coast. In this work, we applied the neo-deterministic seismic hazard analysis (NDSHA) approach to the Alexandria metropolitan area, estimating ground motion intensity parameters, e.g., peak ground displacement (PGD), peak ground velocity (PGV), peak ground acceleration (PGA), and spectral response, at selected rock sites. The results of this NDSHA zonation at a subregional/urban scale, which can be directly used as seismic input for engineering analysis, indicate a relatively high seismic hazard in the Alexandria region (e.g., 0.15 g), and they can provide an essential knowledge base for detailed and comprehensive seismic microzonation studies at an urban scale. Additionally, we established detailed tsunami hazard inundation maps for Alexandria Governorate based on empirical relations and considering various Manning's Roughness Coefficients. Across all the considered scenarios, the average estimated time of arrival (ETA) of tsunami waves for Alexandria was 75–80 min. According to this study, the most affected sites in Alexandria are those belonging to the districts of Al Gomrok and Al Montazah. The west of the city, called Al Sahel Al Shamally, is less affected than the east, as it is protected by a carbonate ridge parallel to the coastline. Finally, we emphasize the direct applicability of our study to urban planning and risk management in Alexandria. Our study can contribute to identifying vulnerable areas, prioritizing mitigation measures, informing land-use planning and building codes, and enhancing multi-hazard risk analysis and early warning systems.

Keywords: multi-scenario hazard analysis; seismic and tsunami hazards; NDSHA; Mediterranean Sea; Alexandria

1. Introduction

Alexandria is a port city on the Mediterranean Sea in northern Egypt. It is one of the world's most important ancient cities. It was founded in 334 BCE (Before the Common Era) by Alexander the Great. It remained the capital of Egypt for almost a thousand years until the Muslim conquest of Egypt in 641 CE (Common Era). Therefore, the city inherited many cultural heritage/historical sites throughout its history, manifested in various monumental and historical sites from different eras (e.g., the Pharaonic, Christian, Romanian, and Islamic Eras). Today, Alexandria has emerged as the second most populous governorate in Egypt, boasting a rich socio-economic and cultural heritage.

The governorate is divided into three cities: Alexandria, Borg Al Arab, and New Borg Al Arab. Alexandria is subdivided into smaller census units, as shown in Figure 1. Alexandria Governorate extends approximately 80 km along the coast of the Mediterranean Sea. It is located hundreds of kilometers south of the Eurasian–African plate boundary. This

plate boundary is characterized by complex geodynamics that trigger large earthquakes and tsunamis. It has several cultural heritage sites with significant historical and cultural value. These sites include, but are not limited to, the Qaitbay Citadel, the Catacombs of Kom El Shoqafa, and the Roman Amphitheater. Protecting these heritage sites from potential hazards such as earthquakes and tsunamis is crucial. In fact, by understanding the specific hazards and their potential impact on cultural heritage, experts can design and implement structural reinforcements, retrofitting measures, and emergency response plans to safeguard these sites.

Alexandria is highly exposed to natural and climate-change-related hazards (e.g., floods, earthquakes, tsunamis, and sea level rise). The city was affected by strong earthquakes and tsunamis throughout its history, causing significant damage and casualties. It is worth noting that highly destructive tsunamis have been reported in some places along the Mediterranean coastline, but only some of them are known and proven to have impacted Alexandria [1–3]. Numerous studies have investigated earthquake [4–8] and tsunami [2,3,9] hazards in Egypt. However, while these studies have focused on individual hazards, it is important to note that some regions are exposed to both risks, necessitating a comprehensive approach to addressing both hazards.

Few studies have been conducted to assess earthquake and tsunami hazards and risks for Alexandria, using either a deterministic or scenario-based approach (e.g., [2,10]) or probabilistic approaches (e.g., [11,12]). Despite the importance and profound challenges faced by the city, detailed joint earthquake and tsunami hazard assessment studies (e.g., earthquake and tsunami) have never been conducted on the city scale. However, it is noteworthy that large offshore earthquakes can be accompanied by tsunamis, as evidenced by historical reports ([5,13] and references therein), geomorphologic studies, and investigations of paleo-tsunami deposits (e.g., [14]), which can have cascading effects. In this current work, we aim to provide a step forward in jointly assessing earthquake and tsunami hazards and risks for Alexandria.

The inadequate understanding of seismic hazards for a given area under urban development may lead to the growth of megacities in seismically active regions with unsafely constructed buildings and infrastructure. Large and even medium-sized earthquakes can cause significant damage in such regions. Seismic hazard studies aim to assess the potential impact of earthquakes, either directly or indirectly, to provide a knowledge base suitable for seismic building codes to guide the design and retrofitting of engineering structures.

The first objective of this work is to conduct a neo-deterministic seismic hazard analysis (NDSHA) at selected sites in Alexandria. The NDSHA methodology (outlined in Section 3.1) incorporates various geological, geophysical, and seismological data, such as earthquake catalogs, focal mechanisms, seismic nodes, seismogenic zones, and subsurface structural models. This study utilizes these data to update the seismic hazard maps for Alexandria and create a dataset of synthetic broadband accelerograms/seismograms. These synthesized records can be directly employed as seismic input for engineering analyses and offer a comprehensive investigation of seismic zoning on an urban scale.

A second, complementary objective is to produce detailed tsunami inundation maps for the Alexandria coastal area. To achieve this, this work was divided into different steps: (a) identifying and extracting from the work of Hassan et al. [3], which contains the last updated maps at the national scale, significant pre-computed earthquake-induced tsunami scenarios in the Eastern Mediterranean that may cause maximum wave amplitude along the Alexandria shoreline; (b) adopting various Manning's Roughness Coefficients (i.e., 0.015, 0.03, 0.05, and 0.08); (c) drawing computed maps with an inundation depth of a 30 m resolution, based on an empirical model that utilizes the maps of average and maximum tsunami wave amplitude provided by Hassan et al. [3], along the Alexandria coastline using QGIS 3.34.11 [15] for spatial analysis and visualization; and (d) producing aggregate maps of the average and maximum tsunami inundation zone.
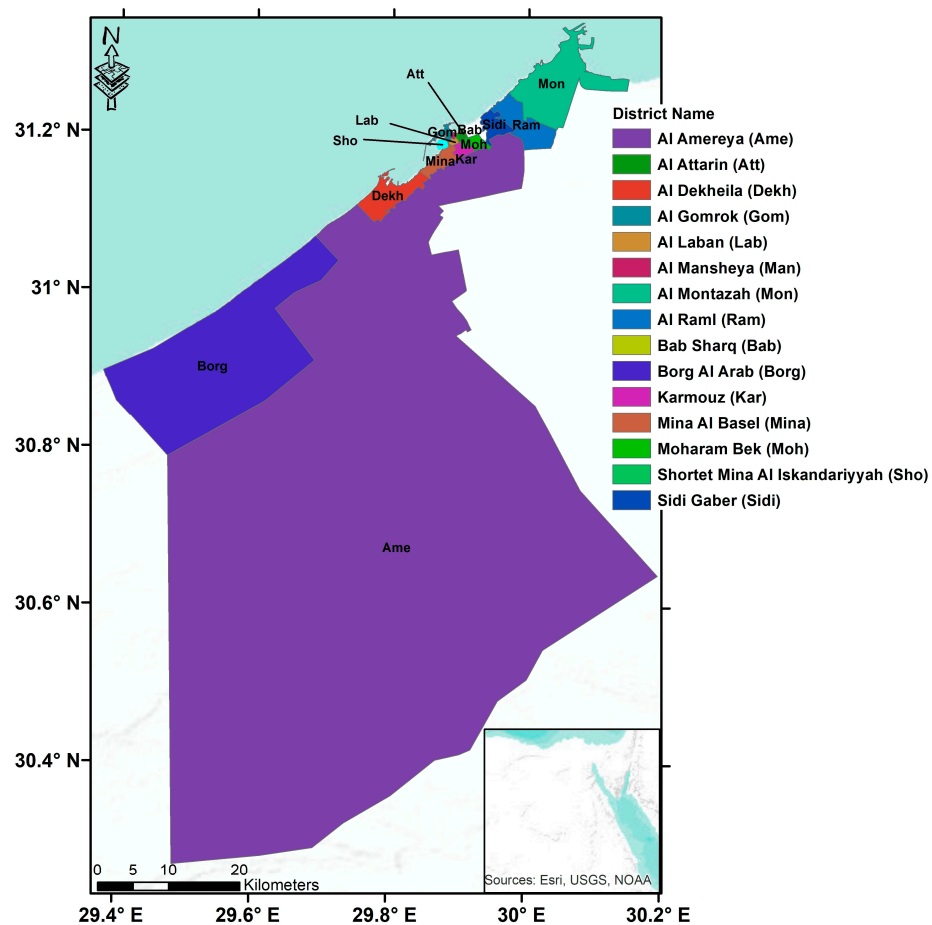
Figure 1. Location map of Alexandria Governorate and main districts (source of census data is the Central Agency for Public Mobilization and Statistics [16]).

Thus, this current work aims to provide a city-scale joint seismic and tsunami hazard analysis, updating and providing detail to some prior studies (i.e., [2,3]). In terms of seismic hazard maps, significant differences arise from the updated earthquake catalog used in this study, which extends to 2020. By contrast, the catalog utilized by Hassan et al. [9] only extends to 2015. Also, the impacts of distant earthquake scenarios, not considered by Hassan et al. [9], on Alexandria are addressed in Section 3.3.

The seismotectonic model employed in this study, differs from the models used in the aforementioned works. Furthermore, the computation in this study was performed at a frequency of 10 Hz, which complements the approach utilized by Hassan et al. [9], with significant variation in the spatial scale of interest and in the methodology employed. In terms of seismic input, this study provides comprehensive information such as peak ground acceleration (PGA), peak ground velocity (PGV), peak ground displacement (PGD), and response spectra for each site in the grid, which has not been previously achieved at this level of resolution Hassan et al. [2] developed tsunami hazard maps for Alexandria based on worst-case scenarios, employing a single scenario for each tsunamigenic source. They also developed an inundation map for Alexandria using a simplified hydrostatic model that did not consider water resistance. Conversely, in this current work, maps of inundation zones were estimated based on the last updated tsunami hazard maps computed along the near shoreline of Alexandria using a multi-scenario approach [3]. Furthermore, various Manning's Roughness Coefficients, i.e., 0.015 for sea floor and open land, 0.03 for thinly populated areas, 0.05 for moderately populated areas, and 0.08 for densely populated areas, were considered. To assess the maps of average and maximum inundation depth at each location, we developed an empirical model that utilizes the tsunami wave height maps in the work of Hassan et al. [3]. Through interpolation, this model provides average and

maximum inundation depth maps on a 30 × 30 m grid. The assignment of these coefficient values was informed by imagery and Google Earth satellite data. GIS data processing and analysis were performed with Quantum GIS (QGIS 3.34.11 [15]).

We emphasize the need for a comprehensive, multi-hazard assessment that considers the interrelationship between seismic and tsunami risks. Our study addresses this gap by employing advanced modeling techniques and high-resolution data to produce detailed hazard maps for Alexandria. We acknowledge the limitations of our study, such as the availability of high-resolution topographic data, current mitigation strategies or defenses for water intrusion, and the focus on rock site conditions, and we discuss potential future research directions to address these limitations. In this current study, we developed, for the first time, high-resolution seismic and tsunami hazard maps jointly for Alexandria, providing a more detailed and accurate assessment of risk. We employed advanced modeling techniques and up-to-date data to produce these high-resolution maps. Our results can be directly applied to urban planning, multi-hazard risk analysis, disaster risk reduction, and coastal resilience strategies in Alexandria.

2. Seismicity, a Seismotectonic Framework, and the Impact of Tsunamigenic Sources on Alexandria

The northern Egyptian continental margin is considered a transitional zone between continental and oceanic crusts, as indicated by [7,17–21]. In this region, the stress field undergoes a shift from predominantly tensional forces on the Egyptian landmass to compressional forces along the Hellenic Arc convergence zone (see Figure 2). The Egyptian continental margin is structurally affected by three main fault trends: northwest–southeast Temsah; northeast–southwest Rosetta, and east–west fault trends (HZ) (e.g., [18,22–24]).

Alexandria is located south of the folded arc that shapes the Mediterranean Ridge [17]. This region's seafloor is occupied by significant geological features, including the Nile Deep Sea Fan, Eratosthenes Seamount, and Herodotus basin [17]. Among these features, the Nile Deep Sea Fan is the most significant accumulation of sedimentary clastic material in the Eastern Mediterranean Sea. Its boundaries are defined by the Dead Sea shear zone to the east, the Cyprus convergent zone, and the Mediterranean Ridge to the north [17]. Several geodynamical studies (e.g., [25,26]) have indicated the northward motion of northern Nubia relative to Eurasia of about 5 mm/yr. Saleh and Becker [27] used crustal deformation data from 16 permanent GPS stations and 47 non-permanent stations that cover Egypt during the period 2006–2012. They estimated the movement rate of northern Nubia and the interaction between the Nubia, Eurasia, and Arabia plates. Their analysis revealed a relative motion between the Nubian and Eurasian plates at a rate of approximately 6.5 ± 1 mm/year, with an increasing trend observed towards the Hellenic trench.

Throughout its history, Alexandria has been subject to varying degrees of damage caused by earthquakes and tsunamis from nearby and distant seismogenic sources. Table 1 indicates the historical and instrumental earthquakes felt in Alexandria that caused considerable damage. Figure 3a,b illustrate the seismic activity around Alexandria during the period from 2000 BCE to 2020 CE [13,17,28–31]. These earthquakes happened at local seismogenic sources (e.g., the continental margin of Egypt) and distant seismogenic sources (e.g., Hellenic and Cyprus Arcs) from Alexandria. Many seismicity studies [12,13,29,31] indicated that there were at least 25 strong earthquakes that impacted Alexandria from 320 to 2020 CE. Historical accounts of the aftermath of the earthquakes in Alexandria indicate widespread devastation, with many houses severely damaged. Tragically, the impact of ground motion and subsequent tsunami inundation resulted in injuries and the loss of thousands of lives [29,32]. The 320, 365, 956, and 1303 CE earthquakes, among others, were severely felt and caused damage and losses in Alexandria due to ground shaking and related tsunamis. Moreover, more recent, some other earthquakes have been felt in Alexandria and have caused some damage (i.e., September 12, 1955, earthquake (6.8 Mw), May 1998 earthquake (5.5 mb), and October 2012 earthquake (5.5 Mw) [13,17,28–30,32–35]). These earthquakes had different epicentral distances, as indicated in Figure 3b, and occurred

at different times, which we believe led to different levels of exposure and vulnerability. Nevertheless, far-source effects, e.g., in connection with the Red Sea earthquakes (e.g., 1969 earthquake, 6.9 Ms) and the Gulf of Aqaba (e.g., 1995 earthquake, 7.3 Mw), were also felt in Alexandria, with a maximum intensity of III-IV on MMS [29].

Table 1. Significant historical earthquakes felt in Alexandria.

Date (CE) Day/Month/Year	Lat°	Lon°	Imax at Alexandria	Magnitude (Mw)
320	31.20	29.90	VI	6.0
21/06/365	35.06	24.94	-	8.3 *
04/796	32.00	31.00	VI	6.0 *
15/09/951	31.00	29.90	V	5.3 *
05/01/956	32.00	30.00	VI	6.0 *
1222	34.7	32.6	-	7.5
08/08/1303	35.20	25.45	VIII	8.5 *
1326	32.00	30.00	V	5.3 *
08/10/1693	32.00	30.50	VI	5.3 *
07/08/1847	29.50	30.50	V	5.4 *
24/06/1870	32.50	30.00	VII	6.8
10/1920	29.40	31.00	-	6.0
30/01/1951	32.40	33.40	-	6.0
24/06/1954	31.50	30.00	-	6.0
28/10/1954	32.40	31.40	-	5.7
12/09/1955	32.50	30.00	VIII	6.8
29/04/1974	30.50	31.70	-	5.4
09/04/1987	32.39	28.97	-	5.1
09/06/1988	32.23	27.90	-	5.3
28/05/1998	31.40	27.67	V-VI	5.3
19/10/2012	32.37	31.25	V	5.5

* Estimated magnitudes are derived using the empirical intensity–magnitude conversion equation developed by Guidoboni et al. [30].

The Eastern Mediterranean (EM) region is a region prone to seismic and tsunami activity, primarily due to the Hellenic Arc. This arc, comprising the West Hellenic Arc (WHA), East Hellenic Arc (EHA), and Cyprian Arc (CA), has been identified as the source of the most significant tsunamis in the region. Historical records, such as the devastating tsunamis of 365 CE and 1303 CE, highlight the potential for destructive tsunamis to impact the Egyptian coast. Studies have shown that large, shallow earthquakes along the Hellenic Arc, particularly those associated with normal and thrust faulting, can trigger significant tsunamis. While the historical record provides valuable insights, the relatively short timeframe limits our understanding of the long-term seismic and tsunami hazard potential of the region.
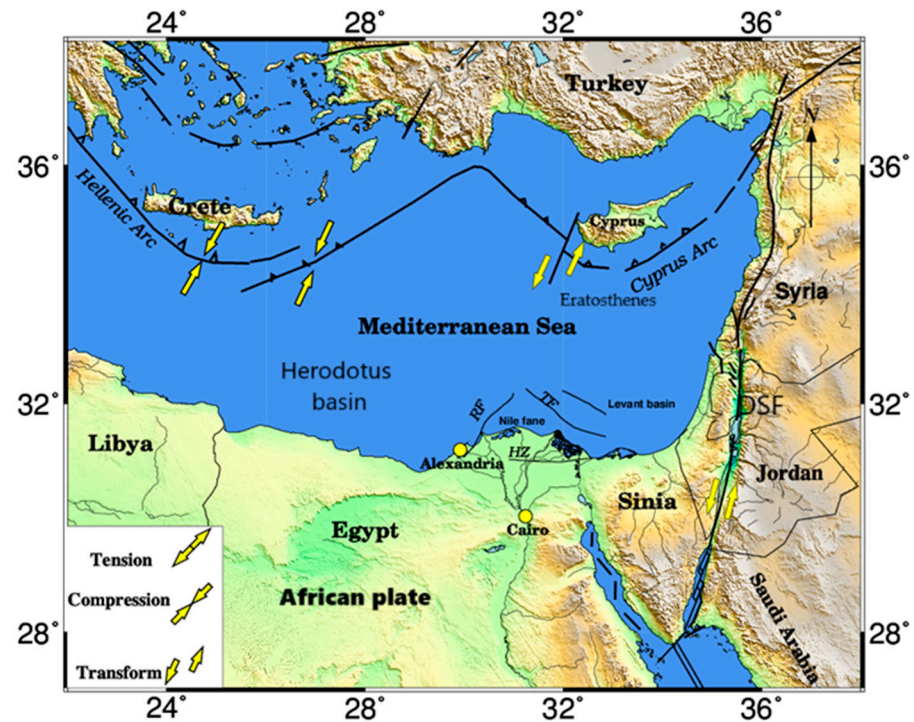
Figure 2. Main tectonic boundaries in the Eastern Mediterranean region, illustrating the Hellenic Arc, Cyprus Arc, Rosetta fault (RF), Temsah fault (TF), and Hinge Zone fault which indicated by the black lines. The small yellow circles indicate the main cities. The yellow arrows indicate present-day stress in and around Egypt and are derived from Ali and Badreldin [31]. Detailed mapping of the fault is derived from [24,36].
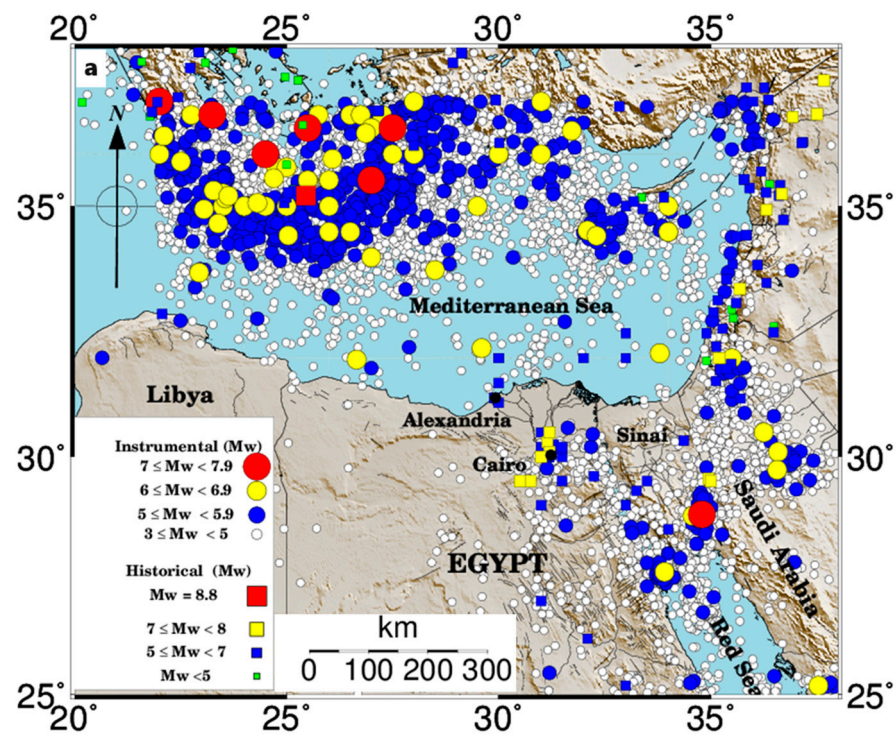

Figure 3. *Cont.*
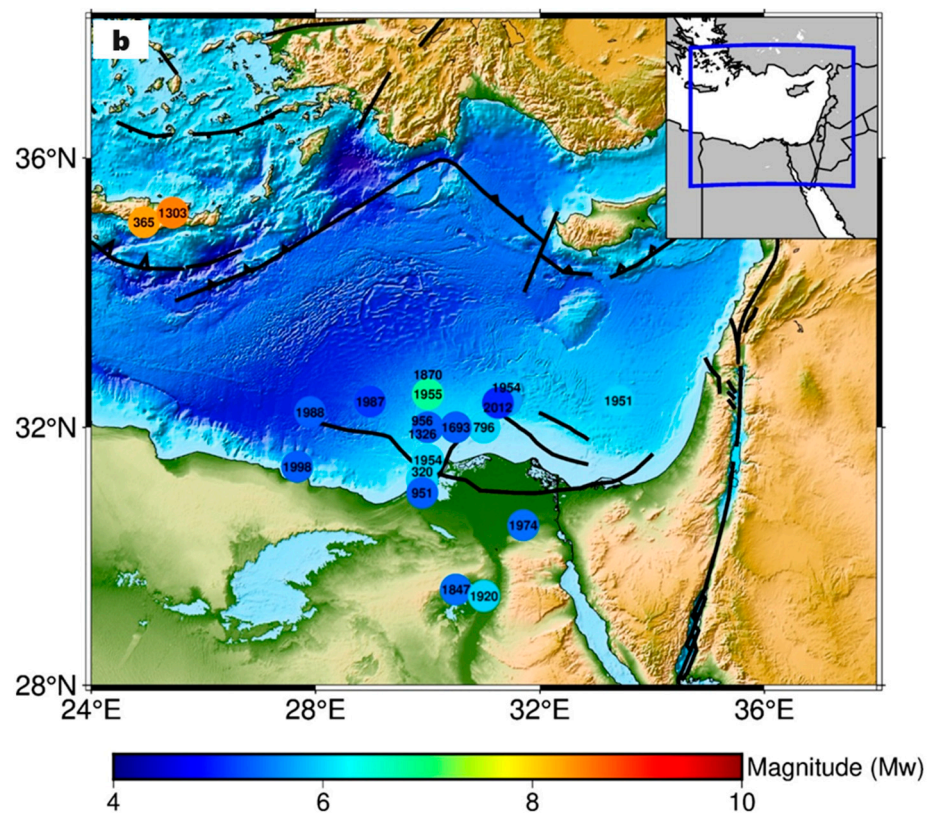
Figure 3. (**a**) Spatial distribution of historical earthquakes (colored squares) from 2000 BCE to 1899 [8,35,37] and regional instrumental seismicity from 1900 to 2020 (colored circles) around Alexandria [8,38]. The location of Alexandria is indicated by the black outlined square and the black lines represent the main tectonic elements in and around Egypt. (**b**) Spatial distribution of significant earthquakes is listed in Table 1.

3. Multi-Scenario Physics-Based Seismic Hazard Analysis

The main target of a seismic hazard study is to estimate the ground motion intensity (e.g., PGA and spectral acceleration (SA) at a given period) for a given area/site of interest. Seismic hazard analysis primarily consists of two steps: (a) characterizing seismic sources of hazard (e.g., sizes and locations of possible earthquakes; (b) characterizing the natural effects of those sources that may result in significant ground motion intensity at a particular location (e.g., [39,40]). In this work, seismic hazard assessment is carried out using the multi-scenario and physics-based methodology known as NDSHA, which has been used for more than two decades (see [41,42]) for a recent review) at regional, national, and local scales. It is worth emphasizing that ground shaking computations within the NDSHA framework are based on multi-scenario physics-based modeling, and therefore no return period is associated with them, unlike standard DSHA and PSHA methods.

The NDSHA method is based on the computation of realistic synthetic time histories of ground motion using basic physical principles of seismic wave generation and propagation in anelastic geo-structural models [43]. It represents a very effective approach, even in regions with incomplete earthquake catalogs available, such as North Africa and Middle Eastern regions [8]. The NDSHA can accommodate any reliable information that enhances hazard understanding and fills knowledge gaps. This includes data from seismogenic nodes derived from morphostructural zonation (MSZ) studies, mechanical models of the lithospheric structure, and paleo-seismological and GPS data (e.g., [44]). This information enables the accurate computation of earthquake ground motion maps, including PGA, PGV, and PGD, or any other seismic engineering parameter extractable from computed synthetic signals (e.g., [2,8]). Also, it may provide a comprehensive dataset of synthetic seismograms,

which is particularly important for the areas that suffer from the endemic lack of proper, strong motion time histories, such as Egypt.

3.1. Data and Methods

In this study, ground motion intensities were derived from broadband time histories computed at the urban scale for a set of selected sites located on a regular grid of approximately $0.1° \times 0.1°$, as depicted in Figure 4. The NDSHA approach used in this study, which has been widely and flexibly used at both regional and urban scales [6,8,10,41,43,45–47], is a physically based approach that simulates potential earthquake ground motions from multi-scenarios. Its suitability for Egypt's complex tectonic setting, limited seismicity record availability, ongoing infrastructure development, and redundancy of historical monuments, makes it a valuable tool for sound seismic hazard assessments (see [43] for a full methodological description).
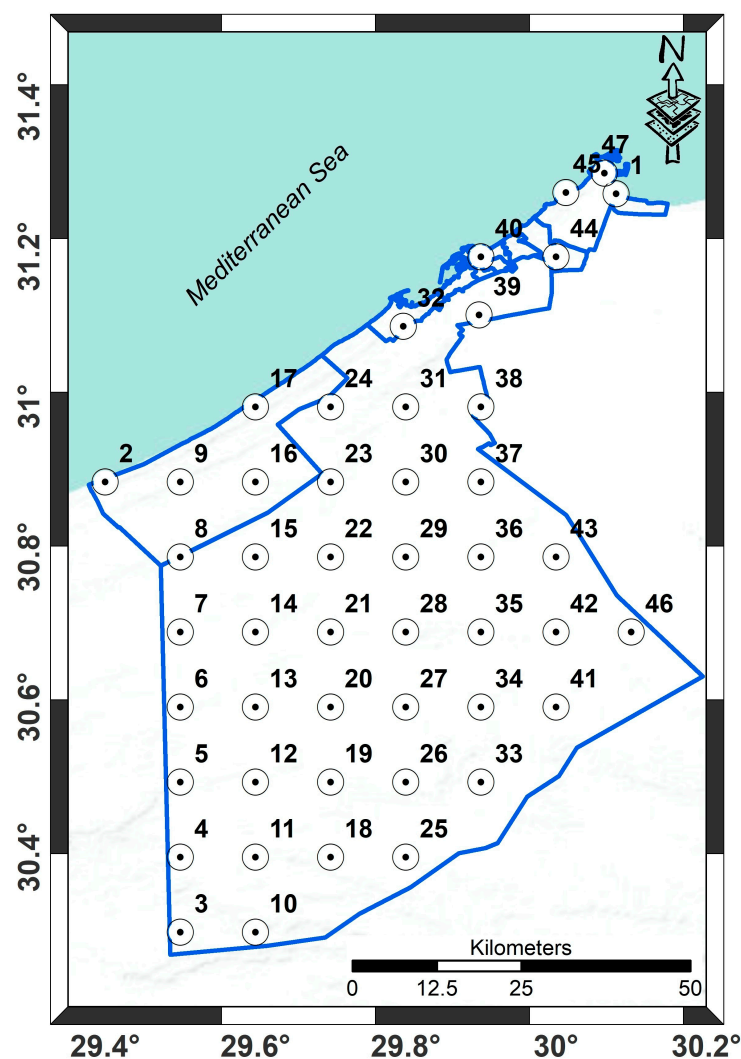
Figure 4. Map of the sites of interest at the city scale, used as observation sites at which seismic hazard parameters are provided Each numbers represent the site number and the blue polygons represent the main districts in Alexandria.

As illustrated in Figure 5, this study incorporates two main components as input for hazard assessment: seismogenic sources (represented by zones and nodes) and crustal structural models for the bedrock. In this work, the NDSHA seismic scenario definition procedure was updated in terms of earthquake catalog, both in time (extended to 2020)

and space (the incorporation of far seismogenic scenarios, as shown in Section 3.3), and seismogenic sources from Hassan et al. [8]. In fact, the seismogenic zones model defined by Hassan et al. [8] was updated to take into account the recent seismic activity in the western region near Alexandria [39], adding seismogenic zone no. 22, as shown in Figure 6.

Also, if the maximum recorded magnitude within the newly delineated seismogenic zone 22 was less than 5, a default magnitude of 5 was assigned, as for each zone, following the NDSHA gridding and smoothing process (see [43] for a complete description). This decision was based on the hypothesis that wherever a seismogenic zone is identified, potentially damaging earthquakes could occur. Conventionally, a magnitude of 5 is considered the lower bound for damaging earthquakes [48], and that is the value adopted as the minimum magnitude threshold for the updated catalog.

Similarly to the work carried out by Hassan et al. [8], we selected the focal mechanism of the most significant event within a specific zone to represent that zone. However, in this study, we carefully examined and revised representative fault plane solutions based on the latest publications on seismic source characterization for Egypt, including recent works [19,31]. Fault plane solutions for significant earthquakes in each seismogenic source were collected and cross-checked between different, previous works. Then, the focal mechanism for the largest magnitude was chosen to represent the present-day dominant tectonic regime of the corresponding seismogenic zone.
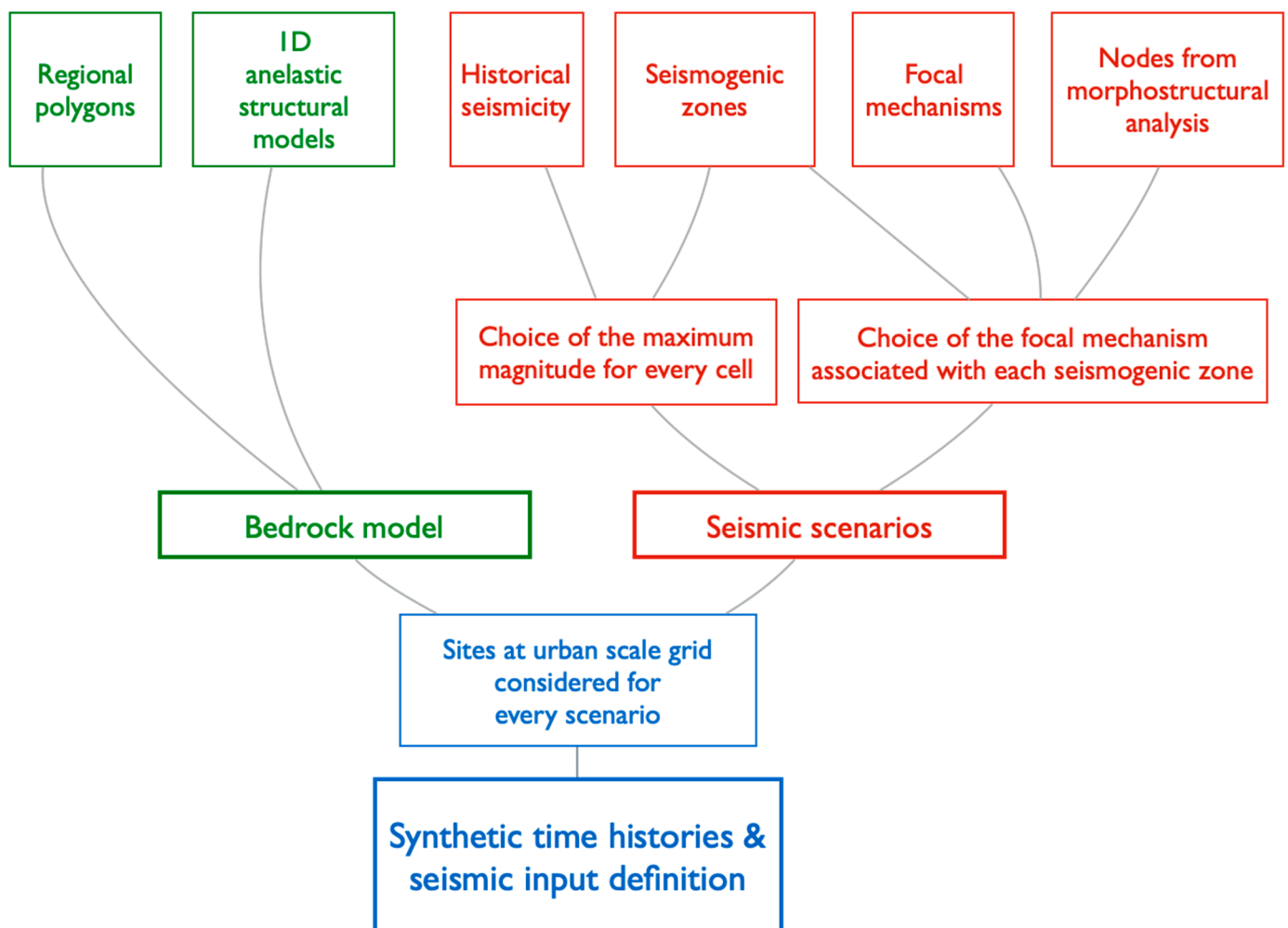

Figure 5. Flow chart of the NDSHA approach adopted for the scale of our analysis.
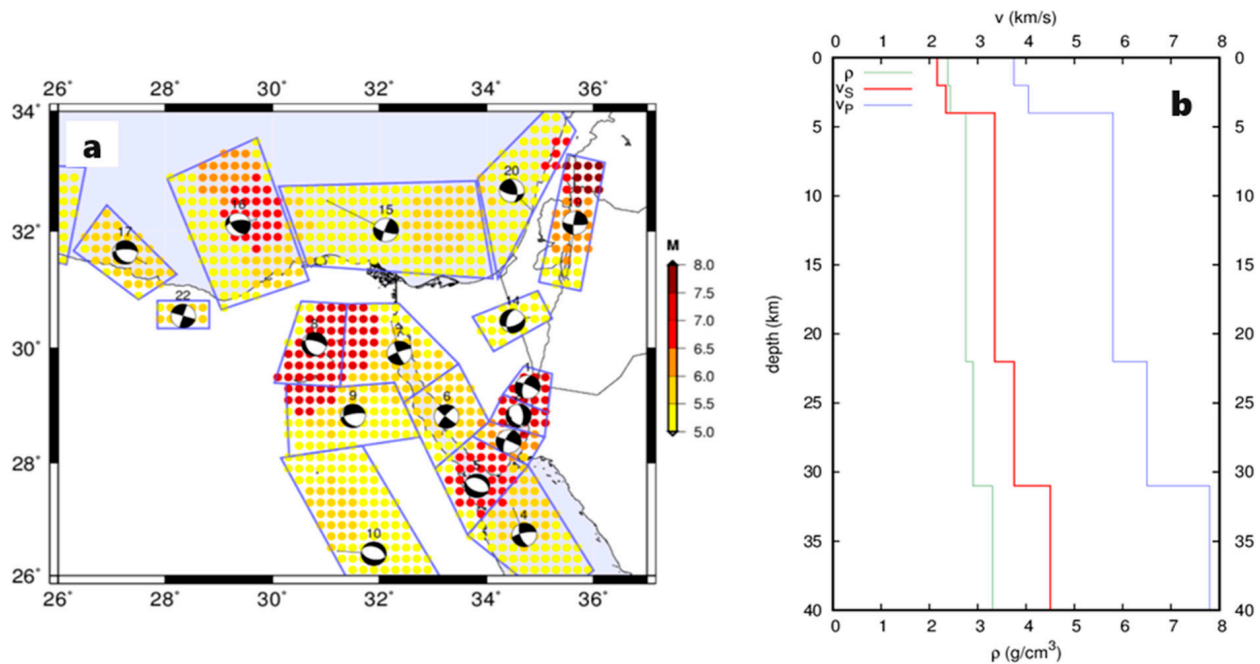
Figure 6. (**a**) Seismogenic zones adopted for computing the NDHSA maps for Alexandria, represented by blue polygons along with their numbers; a representative fault plane solution for each seismogenic source is shown in the center of each source, and the distribution of smoothed seismicity is represented by small circles with different colors according to magnitude. (**b**) Seismic velocities (Vp and Vs) and density (ρ) of the regional bedrock model adopted from El-Sayed et al. [6].

An average bedrock structural model representing the lithospheric properties of the study area was adapted from [6] and used in this study. This model is represented by several flat and anelastic layers with defined thickness, density, P- and S-wave velocities, and attenuation for bedrock conditions at the site of interest (Figure 6). El-Sayed et al. [6] originally derived the 1D-crustal model from deep seismic sounding and Bouguer anomaly profiles published by the Egyptian General Petroleum Company (GAPCO). These datasets are stored in the Atlas of Geology at Cornell University, USA [6]. Physics-based ground motion modeling is currently limited to 10 Hz. Therefore, all ground motion parameters in this study were computed for bedrock conditions for a grid of sites that covers Alexandria at a 10 Hz cut-off frequency. This limitation arises from the need for a more comprehensive understanding of seismic source heterogeneity, the physical properties of rock/soil, and the attenuation parameters, which cannot be realistically resolved at this time. This statement aligns well with the conclusion drawn by Aki [49], who suggested that the field of strong motion seismology does not require the consideration of frequencies higher than approximately 10 Hz.

The NDSHA approach accommodates different magnitude scales from various agencies or magnitude scales assigned to the same event by different authors. To ensure consistency, we homogenized the earthquake magnitudes to moment magnitude (Mw) using the magnitude scaling relationships proposed by Hussein et al. [50]. Additionally, we adopted the magnitude–distance thresholds recommended by Hassan et al. [8] for the computations. We employed smoothing procedures to reduce uncertainty in the location and magnitude of earthquakes. However, relying solely on discretized cells for smoothing often proves insufficient. Therefore, we also evaluated a centered smoothing window, allowing us to analyze earthquake magnitudes in the central cell and neighboring cells. For a more comprehensive understanding of these procedures, refer to the work of Panza et al. [43]. A smoothing procedure for defining earthquake location and magnitude, M, was then applied to account for spatial uncertainty and source extension. After smoothing, only the cells (earthquake sources) located within the seismogenic zones were retained. The

smoothing process makes NDSHA robust and prevents it from possible uncertainties in the earthquake catalog, which is not required to be complete for M < 5.

3.2. Peak Ground Motion Results

Once all the input data and available information for carrying out NDSHA were defined, synthetic seismograms were computed for a set of observation points covering the study area (see Figure 4). The time histories can be directly utilized by engineers as seismic input (e.g., for designing a seismo-resistant structure or evaluating the seismic vulnerability of an existing building) or as a dataset to produce seismic hazard maps of different ground motion intensities. The NDSHA allows for the assessment of seismic hazard in areas with low seismicity and does not have a complete earthquake catalog. The peak ground motion values computed at each site are mapped and shown in Figure 7. The most significant values are concentrated in the northeastern part of the city, which has the maximum acceleration (0.15 g) and velocity (8 cm/s). The estimated high peak acceleration for the sites located in the northeast of Alexandria could be due to the proximity to seismogenic zones and associated seismicity or scenarios located along the continental margin of Egypt, as described in detail in Section 3.1.
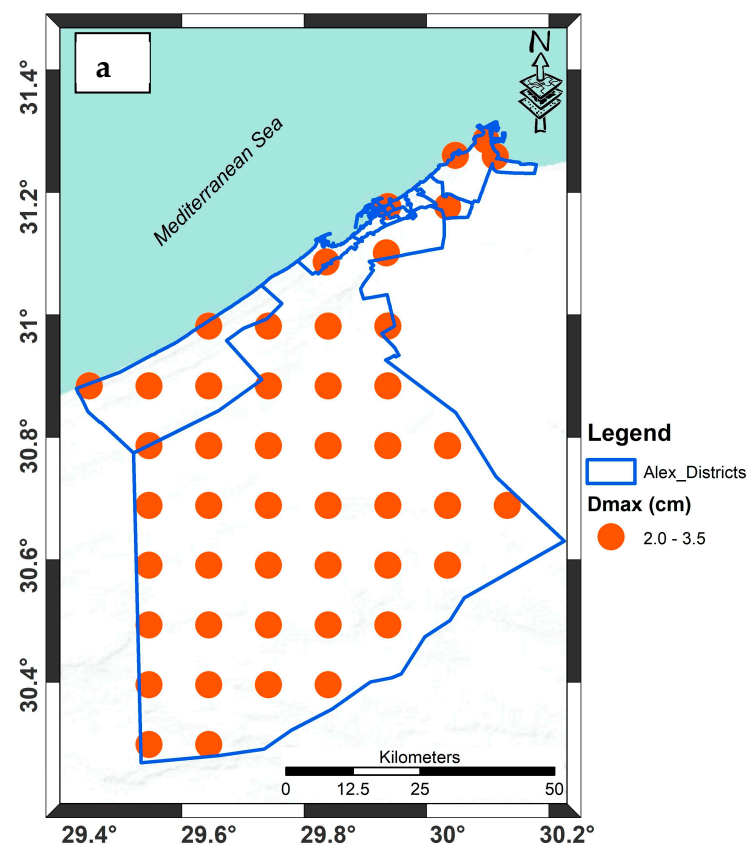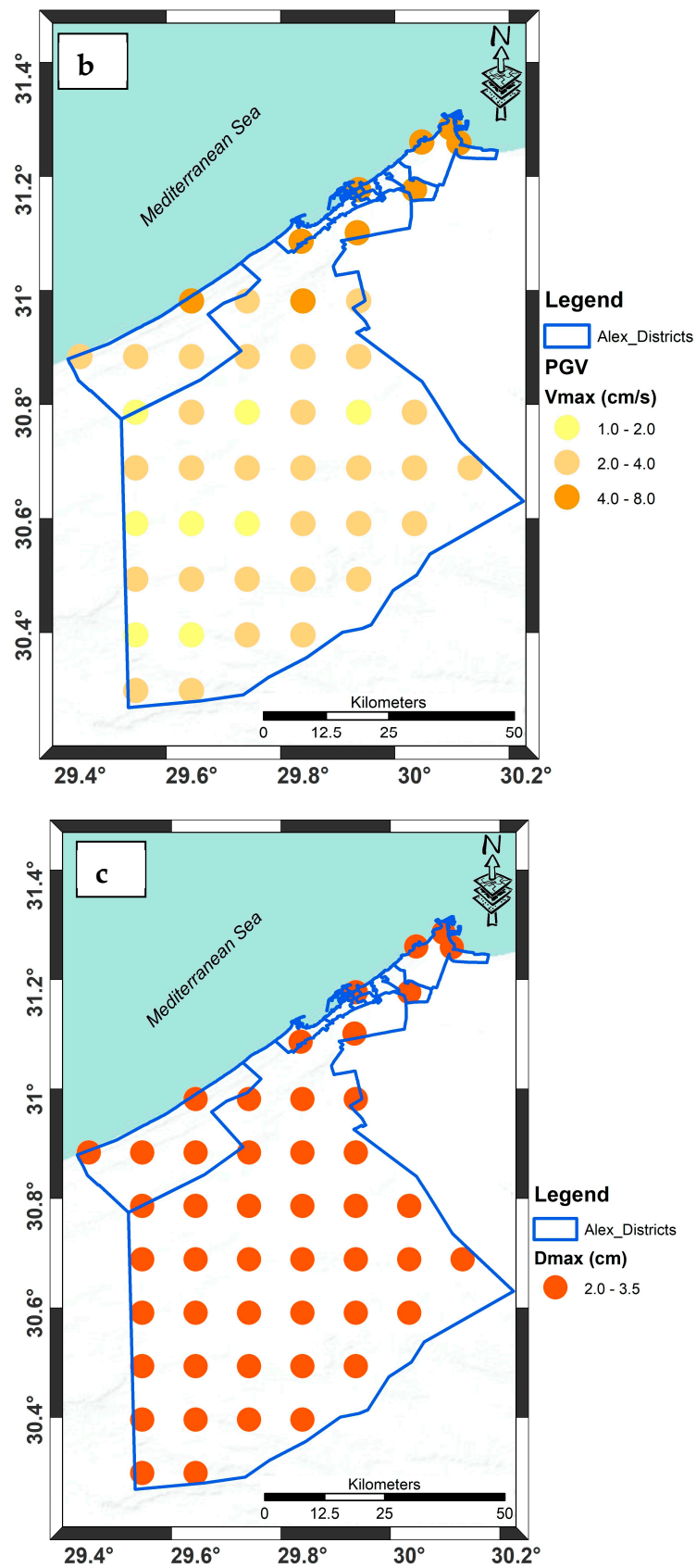

Figure 7. *Cont.*

Figure 7. Maps of: (**a**) peak ground displacement (Dmax); (**b**) peak ground velocity (Vmax) and (**c**) peak ground acceleration (Amax).

3.3. Far Source Effects (Long Period) at Alexandria

Several earthquakes that were felt and that caused damage in Alexandria originated from seismogenic areas outside Egypt (e.g., Hellenic Arc, Cyprus Arc, Gulf of Aqaba, and Dead Sea) [29], as proven from recent and historical observations. The far seismic sources should not be ignored in Alexandria, given their significant magnitude and the frequency content of the ground motion they produce, particularly in the case of tall buildings in the city; the collapse of the Alexandria lighthouse due to the 1375 CE earthquake serves as a well-known example of their potential impact. A long period of ground motion could be hazardous, especially in New Alamein City, which is 35 km west of Alexandria, where many high-rise towers are under construction. Furthermore, strong earthquakes occurring in the Hellenic and Cyprus Arcs may have the potential to cause devastating tsunamis (e.g., 365 Crete earthquake, Mw = 8.5; 1222 Cyprus earthquake, Mw = 7.5; 1303 Rhodes earthquake, Mw = 8.5), as indicated by Hassan et al. [2]. Recent examples are the events of 12 September 1955 (north Egyptian pacific margin, Mw = 6.8), 31 March 1969 (Northern Red Sea, Mw = 6.9), 22 November 1995 (Gulf of Aqaba, Ms = 7.3) and 9 October 1996 (southern Cyprus, Mw = 7.0), which were felt in Alexandria at epicentral distances larger than 300 km [13]. On the other hand, the 320, 365, 956, and 1303 CE events are the most significant historical earthquakes with magnitudes larger than 7. Based on the intensity data and damage pattern information provided by Ambraseys et al. [13] and Guidoboni and Comastri [36] for the 1303 earthquake, El-Sayed et al. [29] suggested that two different earthquakes hit the city on the same day—one earthquake from a local source (Al Fayoum area) and another earthquake from a far event located in the Hellenic Arc. They supported this suggestion by attributing the collapse of the top of the ancient lighthouse of Alexandria, the slow ground motion that made people walk with difficulties, and the duration of shaking that lasted for several minutes to the long period effect from the far source, which nucleated in the Hellenic Arc. The local event was suggested to be in El-Fayoum, which caused short-period effects to be reported, e.g., the complete and heavy damage reported in Cairo and Nile Delta, including the public buildings that were usually of good quality, the way people felt the earthquake, the movement of the water in the Nile, and the rock falling and landslides near Minya.

The ground motion intensities (e.g., PGA, PGV, and PGD) were computed for the 1303 earthquake in order to investigate and verify whether the strong earthquakes that originated in the Hellenic Arc could significantly cause damage in Alexandria. According to Ambraseys et al. [16] and Guidoboni and Comastri [35], the August 1303 earthquake, with $I_0 = X$ Mw = 8.5, originated in the Hellenic Arc 600 km away from the Egyptian coasts at 25.63° E and 35.18° N, which caused widespread damage in the Eastern Mediterranean region. The 1D-crustal modal (Figure 6) and source parameters of 1303 earthquakes, which are listed in Table 2, were used to compute the synthetic seismograms at Alexandria. The shaking lasted more than 4 min, and the computed peak ground motion at Alexandria was 6 cm/s^2, 4 cm/s, and 18 cm for PGA, PGV, and PGD, respectively. Based on these results, we can support part of the conclusions by El-Sayed et al. [29], who proposed that the reported damage in Egypt was related to a local earthquake.

Table 2. Source parameters of the August 1303 earthquake [35].

Epicenter (Lon, Lat)	(25.63°, 35.18°)
Magnitude	8.5 Mw
Hypocentral depth	20 km
Ep. distance from Alexandria	609 km
Strike, dip, rake	115°, 45°, 110°

3.4. Maximum Credible Seismic Input (MCSI)

The MCSI response spectrum is calculated based on the methods described by Rugarli et al. [51]. Multiple rupture scenarios are considered stochastic realizations for each seismogenic source, which are defined in terms of magnitude, location, and focal mechanism.

Spectral acceleration values (SA) are computed at various periods (0–4.0 s), and the maximum median value is selected, as illustrated in Figure 8a–d. In such a way, the MCSI represents a reliable estimation of the upper-bound level of shaking that could occur at a selected site (not considering their probability of occurrence), usefully summarizing the information contained in the multitude of time histories considered in the NDSHA for engineering analysis.
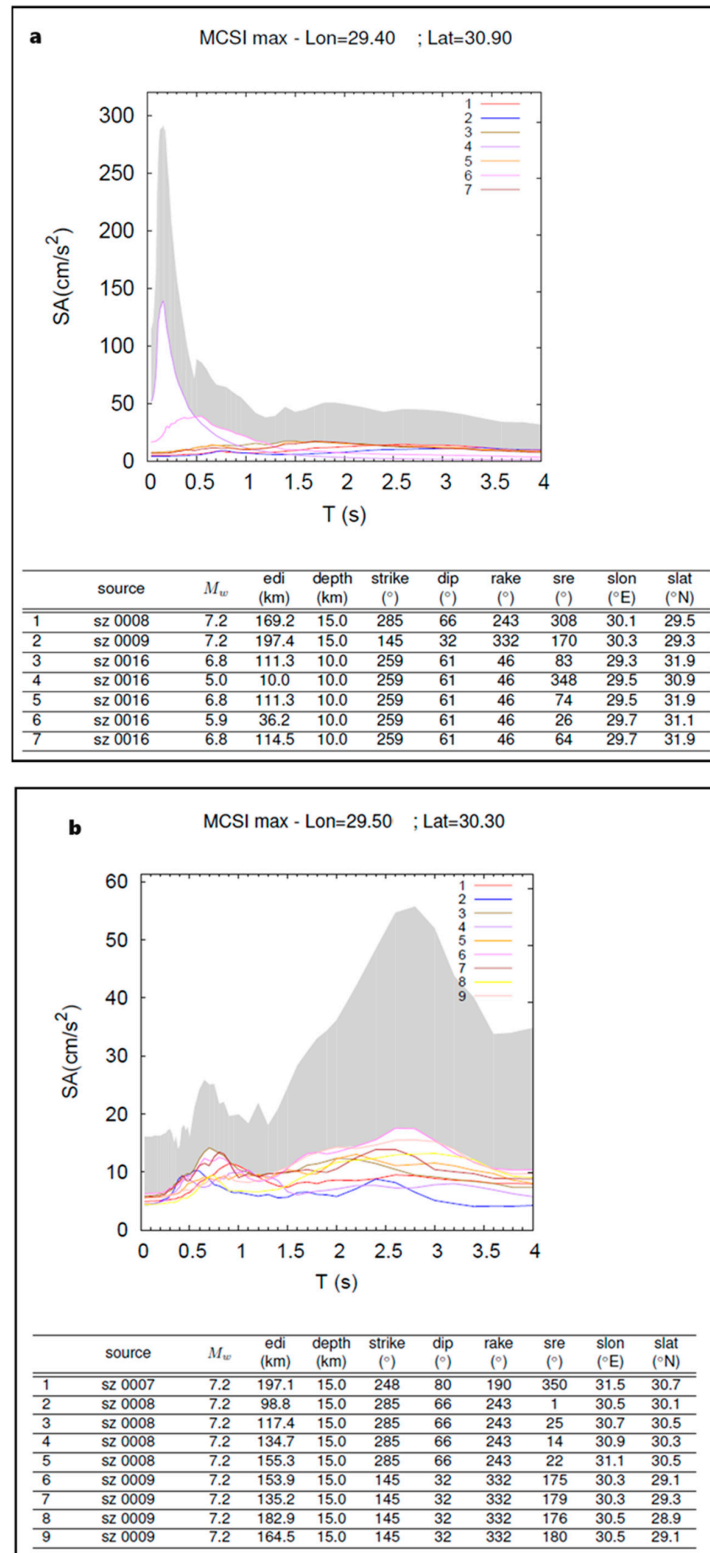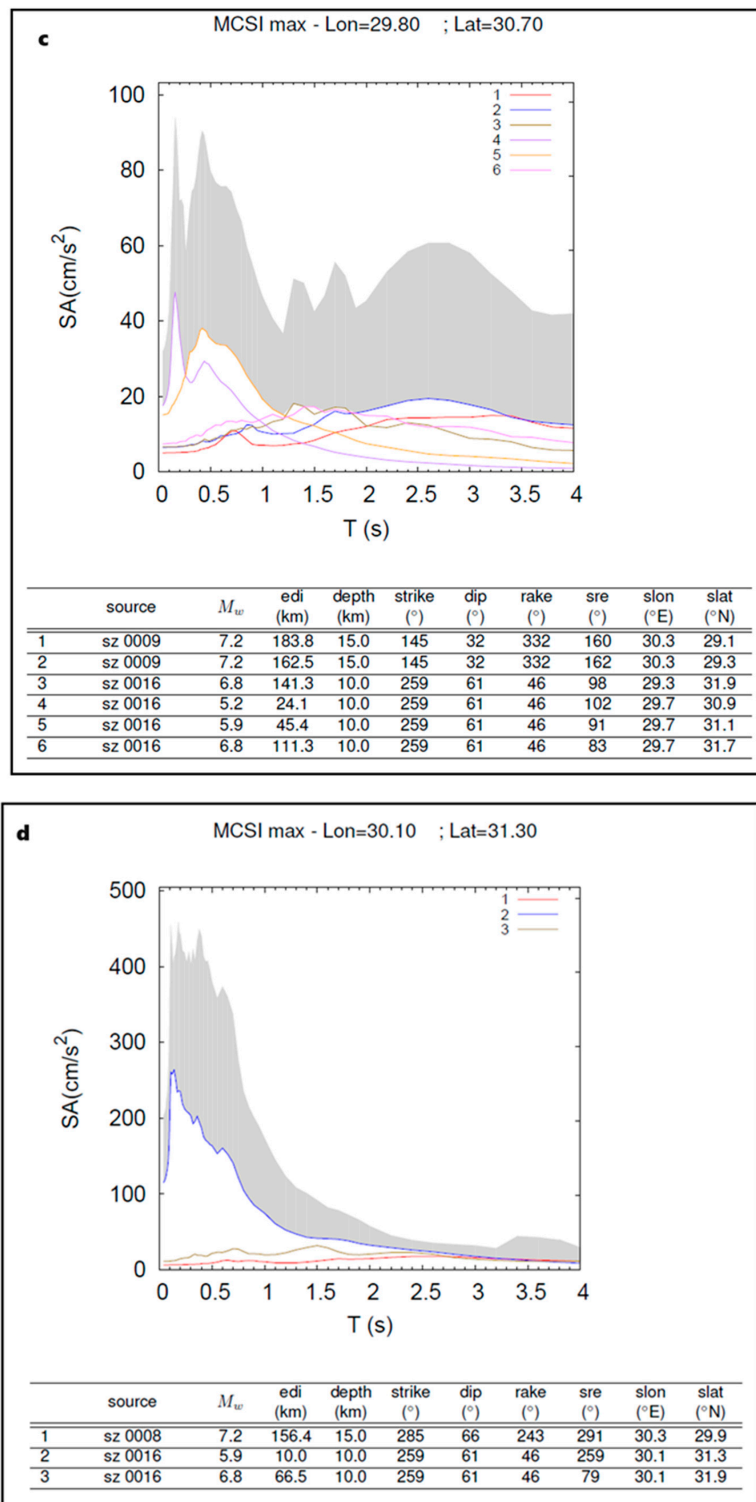

a MCSI max - Lon=29.40 ; Lat=30.90

	source	M_w	edi (km)	depth (km)	strike (°)	dip (°)	rake (°)	sre (°)	slon (°E)	slat (°N)
1	sz 0008	7.2	169.2	15.0	285	66	243	308	30.1	29.5
2	sz 0009	7.2	197.4	15.0	145	32	332	170	30.3	29.3
3	sz 0016	6.8	111.3	10.0	259	61	46	83	29.3	31.9
4	sz 0016	5.0	10.0	10.0	259	61	46	348	29.5	30.9
5	sz 0016	6.8	111.3	10.0	259	61	46	74	29.5	31.9
6	sz 0016	5.9	36.2	10.0	259	61	46	26	29.7	31.1
7	sz 0016	6.8	114.5	10.0	259	61	46	64	29.7	31.9

b MCSI max - Lon=29.50 ; Lat=30.30

	source	M_w	edi (km)	depth (km)	strike (°)	dip (°)	rake (°)	sre (°)	slon (°E)	slat (°N)
1	sz 0007	7.2	197.1	15.0	248	80	190	350	31.5	30.7
2	sz 0008	7.2	98.8	15.0	285	66	243	1	30.5	30.1
3	sz 0008	7.2	117.4	15.0	285	66	243	25	30.7	30.5
4	sz 0008	7.2	134.7	15.0	285	66	243	14	30.9	30.3
5	sz 0008	7.2	155.3	15.0	285	66	243	22	31.1	30.5
6	sz 0009	7.2	153.9	15.0	145	32	332	175	30.3	29.1
7	sz 0009	7.2	135.2	15.0	145	32	332	179	30.3	29.3
8	sz 0009	7.2	182.9	15.0	145	32	332	176	30.5	28.9
9	sz 0009	7.2	164.5	15.0	145	32	332	180	30.5	29.1

Figure 8. *Cont.*

MCSI max - Lon=29.80 ; Lat=30.70

	source	M_w	edi (km)	depth (km)	strike (°)	dip (°)	rake (°)	sre (°)	slon (°E)	slat (°N)
1	sz 0009	7.2	183.8	15.0	145	32	332	160	30.3	29.1
2	sz 0009	7.2	162.5	15.0	145	32	332	162	30.3	29.3
3	sz 0016	6.8	141.3	10.0	259	61	46	98	29.3	31.9
4	sz 0016	5.2	24.1	10.0	259	61	46	102	29.7	30.9
5	sz 0016	5.9	45.4	10.0	259	61	46	91	29.7	31.1
6	sz 0016	6.8	111.3	10.0	259	61	46	83	29.7	31.7

MCSI max - Lon=30.10 ; Lat=31.30

	source	M_w	edi (km)	depth (km)	strike (°)	dip (°)	rake (°)	sre (°)	slon (°E)	slat (°N)
1	sz 0008	7.2	156.4	15.0	285	66	243	291	30.3	29.9
2	sz 0016	5.9	10.0	10.0	259	61	46	259	30.1	31.3
3	sz 0016	6.8	66.5	10.0	259	61	46	79	30.1	31.9

Figure 8. MCSI response spectra at four selected sites: 2 (**a**), 3 (**b**), 28 (**c**) and 47 (**d**). The gray band represents the MCSI, as defined by Rugarli et al. [51], which is controlled (at various periods) by the sources reported and described in each of the underlying tables. Each colored line represents a response spectrum for an earthquake scenario that contribute to the MCSI response spectra, and each source parameter is indicated in the table below the graph. The tables below the graphs show different seismogenic source numbers affecting the selected site, along with its magnitude (Mw), epicentral distance (edi), depth, strike, dip, rake, source receiver angle (sre), site longitude (slon), and site latitude (slat). The solid line represents the median, and the shaded area shows the 95th percentile (i.e., median + 2σ).

In this study, the MCSI was computed at bedrock (i.e., soil class A with $Vs_{30} \geq 800$ m/s, according to Eurocode 8 [52], with a 10 Hz cutoff frequency for the sites shown in Figure 4. Due to the complexity of the rupture process on a fault (and the implicit impossibility to deterministically predict a future one), one hundred kinematic realizations were considered in the analysis. An example of the results is shown in Figure 8, where the MCSI evaluated at selected sites (i.e., [2,3,23,42]) along the shoreline of Alexandria are shown, with the median and 95th percentile.

For site 47 (Figure 8d), three seismogenic sources contribute to its MCSI, and the maximum spectral acceleration is 0.27 g and 0.45 g for median and median + 2σ, respectively, at a 0.2 s spectral period. The maps with the maxima MCSI spectral acceleration values (95th percentile) at two selected periods (T = 0.5 s and T = 1.0 s) for the considered sites are shown in Figure 9.
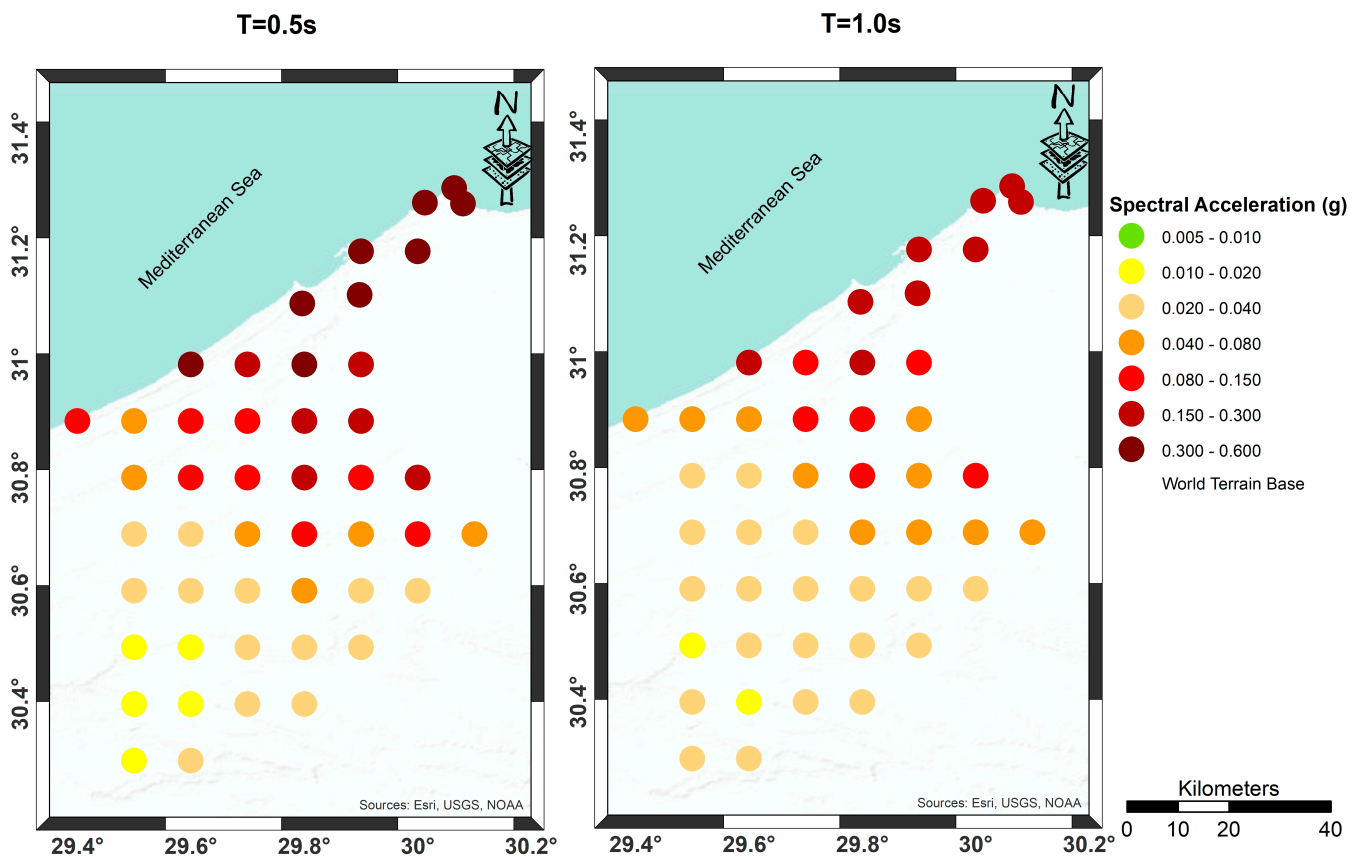
Figure 9. Maxima MCSI spectral acceleration values (95th percentile) at the periods T = 0.5 s and T = 1.0 s for the studied sites.

4. Multi-Scenario Physics-Based Tsunami Hazard Analysis: Data and Methods

Highly destructive tsunamis were reported at some locations along the Mediterranean Sea coastline. However, only a few have been identified as affecting Alexandria Governorate on Egypt's north shore [1,53]. The most hazardous tsunami events known to affect Alexandria originated at the Hellenic and Cyprian Arcs, since they are defined as tsunamigenic sources or capable of generating tsunamis. Some of the tsunamigenic earthquakes generated along these well-known seismogenic sources (e.g., 365, West Crete tsunami Mw = 8.3, 1222, Cyprus tsunami Mw = 7.5, 1303, East Crete Mw = 8.5) were documented in historical diaries and geomorphological and geological records for certain locations along the Egyptian coastline. Previous studies [3,9,13] provide evidence of these events. Those tsunamigenic earthquakes caused destruction and fatalities in Alexandria (e.g., [13]). In addition, recent tsunami hazard studies, based on either probabilistic assessment (2475-year return period) or numerical simulations (e.g., TSUMAPS-NEAM [54,55], indicate that a

maximum tsunami wave amplitude of 6 m along the coast could be expected. More recent tsunami events (e.g., 2 May 2020, South Crete Mw = 6.7 [3]; the Izmir-Samos in 30 October 2020, Mw = 6.6 [56], and Bodrum-Kos on 20 July 2017 with Mw = 6.6 [57]) include small local tsunamis that might motivate us to evaluate existing early warning systems, emergency and evacuation plans, and tsunami hazards and their associated risks in order to achieve the desirable, proper, and sustainable management of the Mediterranean coastline.

In this study, we generated inundation zone maps utilizing the most recent tsunami hazard maps, which were created using a multi-scenario approach along the shoreline of Alexandria at various points of interest [3]. We considered different Coefficients values, of 0.015, 0.03, 0.05, and 0.08, corresponding to the seabed, open land, sparsely populated areas, moderately populated regions, and densely populated zones, respectively. To evaluate the average and maximum inundation depths for each location, we developed an empirical model based on the tsunami wave height maps presented by Hassan et al. [3]. This model employs interpolation techniques to produce maps of average and maximum inundation depths on a 30 × 30 m grid. The assignment of coefficient values was informed by satellite imagery and data from Google Earth. GIS data processing and analysis were carried out using Quantum GIS (QGIS 3.34.11 [15]).

4.1. Tsunamigenic Earthquake Sources in the Eastern Mediterranean

The Eastern Mediterranean basin (EM) is a small oceanic basin renowned for its intricate tectonic characteristics. Geodynamical studies on the EM basin widely agree that the African plate subducts beneath Eurasia along the Hellenic Arc (HA) at a rate of approximately 1 cm/year [58]. In the northern section of the Mediterranean basin, the Aegean Sea is recognized as an extensional basin, with an opening rate of around 4.0 cm/year [59]. Moving towards the eastern part of the EM, the collision between the African plate and the Anatolia micro-plate occurs along the Cyprian Arc (CA) at a rate of 6 mm/year [59]. The ongoing conversion between African and Eurasian plates has been evidenced in both arcs using bathymetry, seismicity, and other geophysical data. From the available historical tsunami catalog, it appears that earthquakes and submarine landslides are the two primary tsunamigenic sources in the EM followed by volcanic eruptions [2]. Several tsunamis may have originated as a combination between the two different sources. Based on the spatial distribution of seismicity, tsunami activity, and present-day tectonic activity, many authors (e.g., [60]) have divided the EM into three different tsunamigenic sources, i.e., the West Hellenic (WHA) and East Hellenic (EHA) Arcs and the Cyprian Arc (CA), arranged from west to east (Figure 10). Evidently, most if not all seismotectonic studies (e.g., [60,61]) have concluded that the WHA, EHA, and CA are the sources of worst-case scenarios as concerns sustainable development planning along the Alexandria coastline. According to the historical record of earthquakes (e.g., [13,62]), the Hellenic Arc can be considered the source that generated the strongest earthquakes and basin-wide tsunamis that have occurred in the EM so far. Its tsunamis are considered the most hazardous source for the EM, and they are well known to produce significant destruction along the Egyptian coast, particularly the tsunamis of 365 CE and 1303 CE. The Hellenic Arc's tsunamis are generated due to the occurrence of large shallow earthquakes of vertical displacement. Many studies have discussed the history of earthquakes and tsunamis in the Hellenic Arc and evaluated their potential to generate future activities. For example, Galanopoulos [63], Papadopoulos and Chalkis [64], and Papazachos et al. [65] investigated tsunamis along the Greek coasts. Papazachos and Dimitriu [66] found that the most devastating tsunamis occurred in areas of shallow normal and thrust faulting. Papadopoulos et al. [61] found that about 18 tsunamis are documented in the EHA.

Table 3. Seismological parameters of earthquake scenarios adopted in this work.

Scenario No	Lat°	lon°	Magnitude (Mw)	Depth [km]	Strike°	Dip°	Rake°	Legnth [km]	Width [km]	Slip (m)
S1	34.79	23.90	8.5	45	326	30	90	100	75	20
S2	34.51	24.01	8.5	45	326	35	90	170	75	20
S3	36.50	21.66	8.5	45	326	30	90	175	75	20
S4	35.57	22.77	8.5	45	326	30	90	150	75	20
S5	34.09	24.78	8	45	250	30	90	90	47	20
S6	34.79	26.85	8	45	250	30	90	122	47	20
S7	35.01	28.23	8	45	250	30	90	100	47	20
S8	36.61	28.71	8	40	250	35	90	100	47	90
S9	34.23	33.51	8	5	280	20	90	100	46.7	8
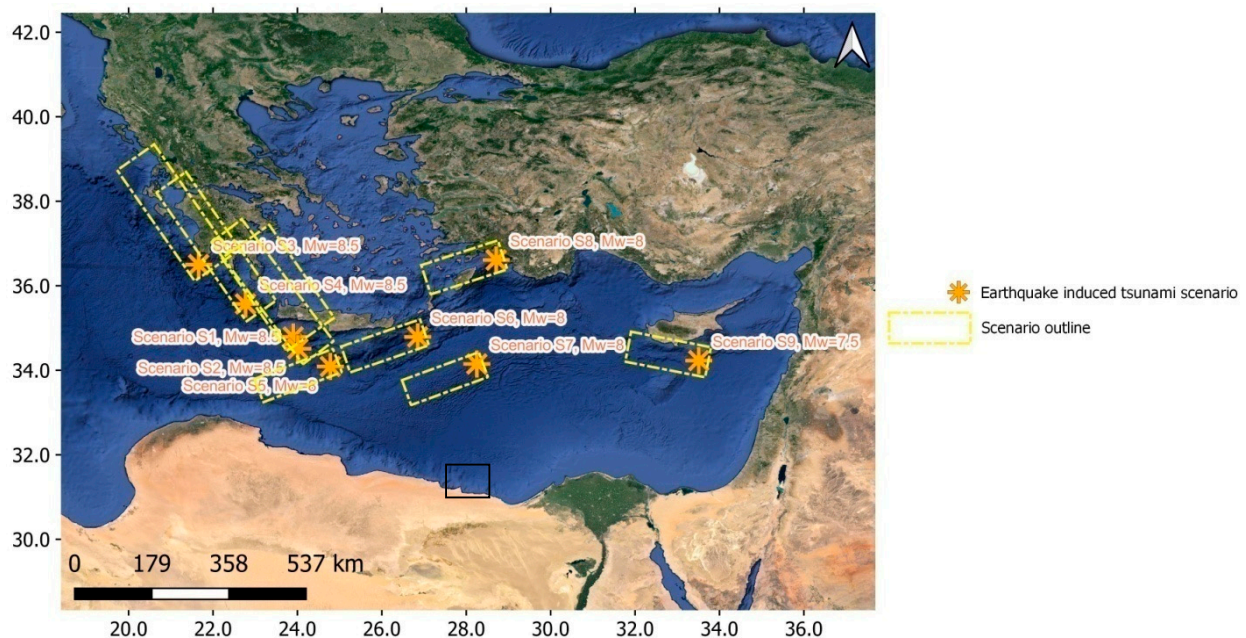
Figure 10. Nine seismogenic/tsunamigenic source models in the Eastern Mediterranean region compiled from the DISS-3.3 [67] database and individual studies adopted for tsunami hazard assessment extracted from Hassan et al. [3] and adopted in this work, as shown in Table 3 [68] (last access: January 2023). The black square polygon defines the area of interest, while the yellow polygon forms the tsunamigenic source models/scenarios.

The Cyprian Arc is the closest collision zone to the Egyptian coast but is smaller, slower, and less active than the HA. Large earthquakes triggering local to regional tsunamis in the Cyprian Arc had happened throughout history, but so far no significant basin-wide tsunami is known to have originated in this source due to its relatively small magnitude relative to the Hellenic Arc.

4.2. Selected Tsunami Scenarios for Alexandria

The uncertainty in the locations and magnitudes of the causative earthquakes represent the main obstruction for assessing tsunami hazards in the EM. Consequently, the region has a wide range of potential earthquake-induced tsunami scenarios (e.g., [60,68,69]). England et al. [70] have indicated that the two most devastating historical tsunamis recorded in the region, those of 365 and 1303, were probably generated by strong earthquakes at the Hellenic plate boundary, and there is strong evidence for them, as discussed in

the Introduction section, with references available. However, there is no clear evidence from seismology alone for the existence of the faults that slipped in the tsunamigenic earthquakes of 365 or 1303. Therefore, these reasons motivated England et al. [70] to develop a seismogenic source model that took advantage of recent understanding of the tsunami hazard at this plate boundary, which was developed by combining geological, geophysical, geodetic, geomorphological, geochronological, and historical data. To achieve the aim of this study, we selected eight source models (i.e., scenarios S2 to S9) adopted in the work of Hassan et al. [3], while S1 was taken from the DISS-3.3 [68] database. These selected scenarios represent the most significant ones responsible for the maximum tsunami wave amplitude in the Alexandria coastline. These sources are reproduced, and their details are presented in Table 3 and Figure 11.
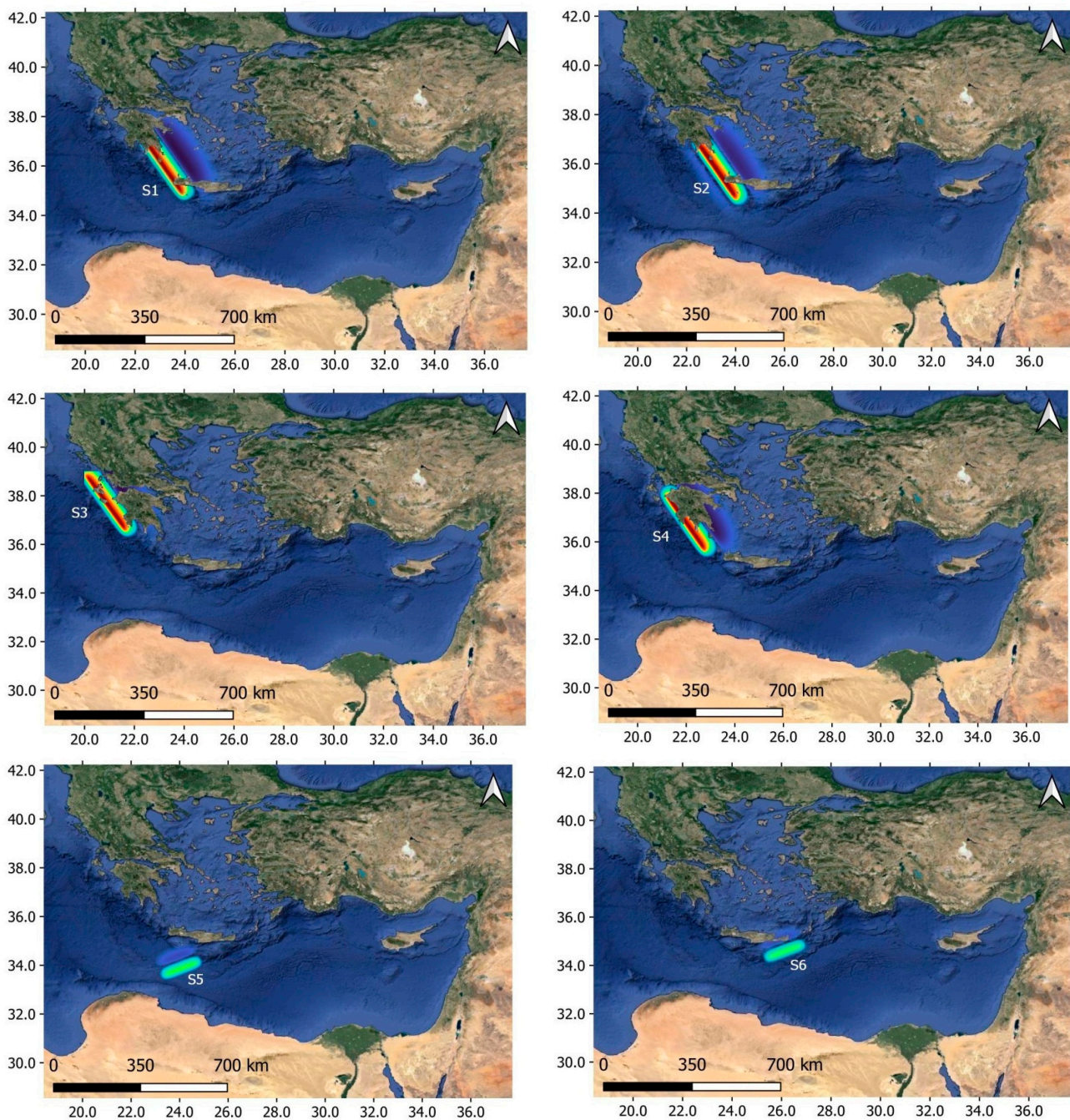
Figure 11. *Cont.*
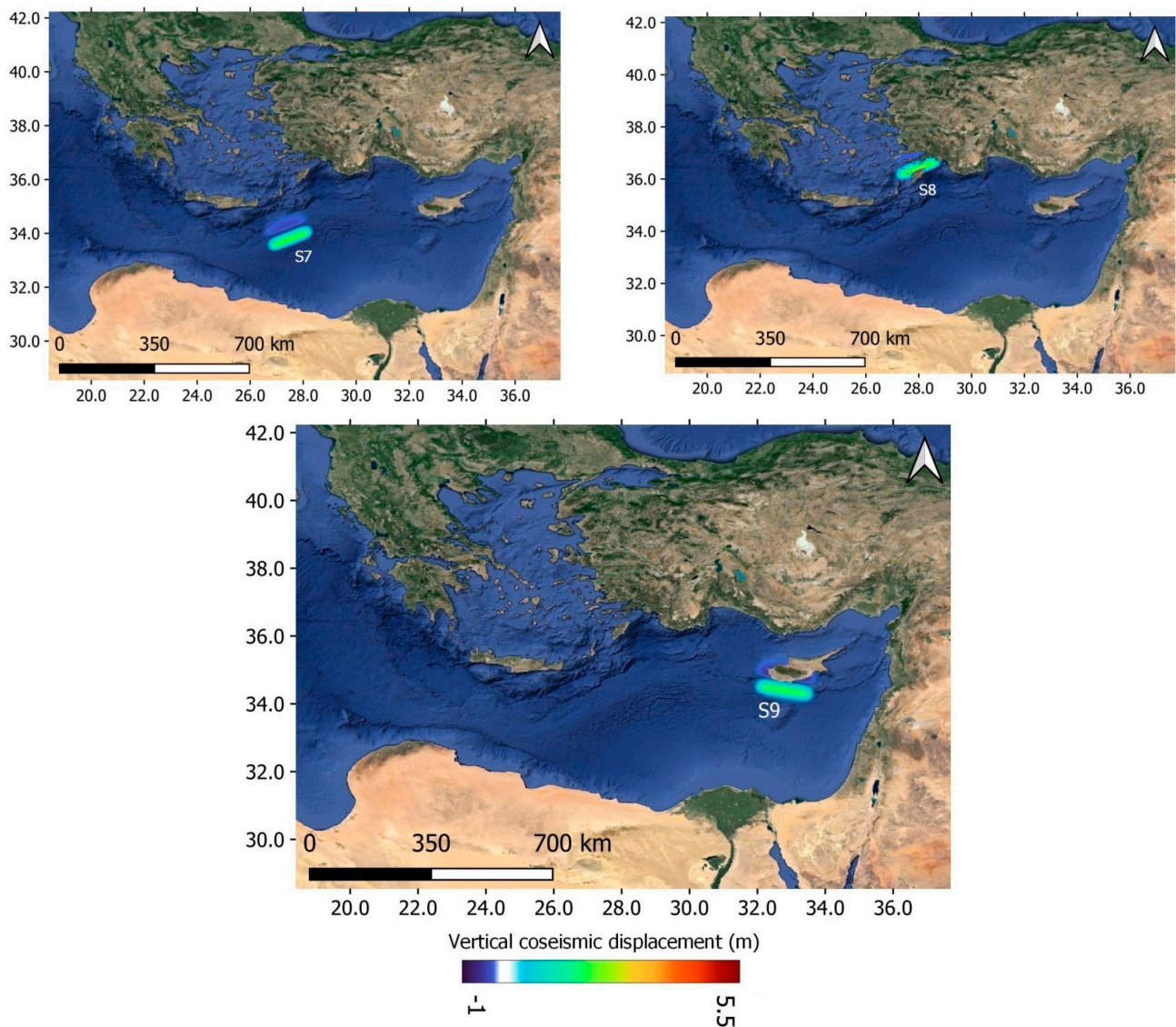
Figure 11. Initial tsunami conditions (coinciding with the vertical coseismic displacement of the seabed) for the nine selected earthquake model scenarios from Hassan et al. [3]; the red and blue colors indicate positive and negative seawater elevations, respectively.

4.3. Tsunami Hazard Maps for Alexandria

Figure 12 shows maps of mean and maximum estimated tsunami wave amplitude values from aggregated tsunami scenarios for Alexandria, as described in Section 4.2. It quite clear that scenarios S6 and S7, which are situated in the EH part, are the most severe scenarios that could produce the highest hazard in terms of tsunami wave amplitude and inundation distance to the Alexandria coastal zone, with an estimated maximum tsunami wave amplitude of 6.0–6.5 m (±mean sea level), whereas the estimated mean of the maximum wave amplitude of all individual scenarios is about 2.5–3.0 m (Figure 12). In this work, an aggregated scenario was built using the maximum and mean tsunami wave amplitude values estimated (Figure 12) through the combining or aggregating of selected individual scenarios listed in Table 3. The aggregated scenario for Alexandria was established by merging all wave tsunami amplitude values estimated at each site along the coast in one feature class using a geographic information system (GIS) tool, and then the highest values were retained. This maximum estimated tsunami wave amplitude from individual scenarios is registered at the western coastline of the governorate. The maps of average ETA for Hellenic and Cyprus Arc scenarios are mapped and shown in Figure 13.

The average ETA defined from all individual scenarios for Alexandria shorelines ranges between 75 and 80 min (Figure 13) for both the Hellenic and Cyprus Arcs.
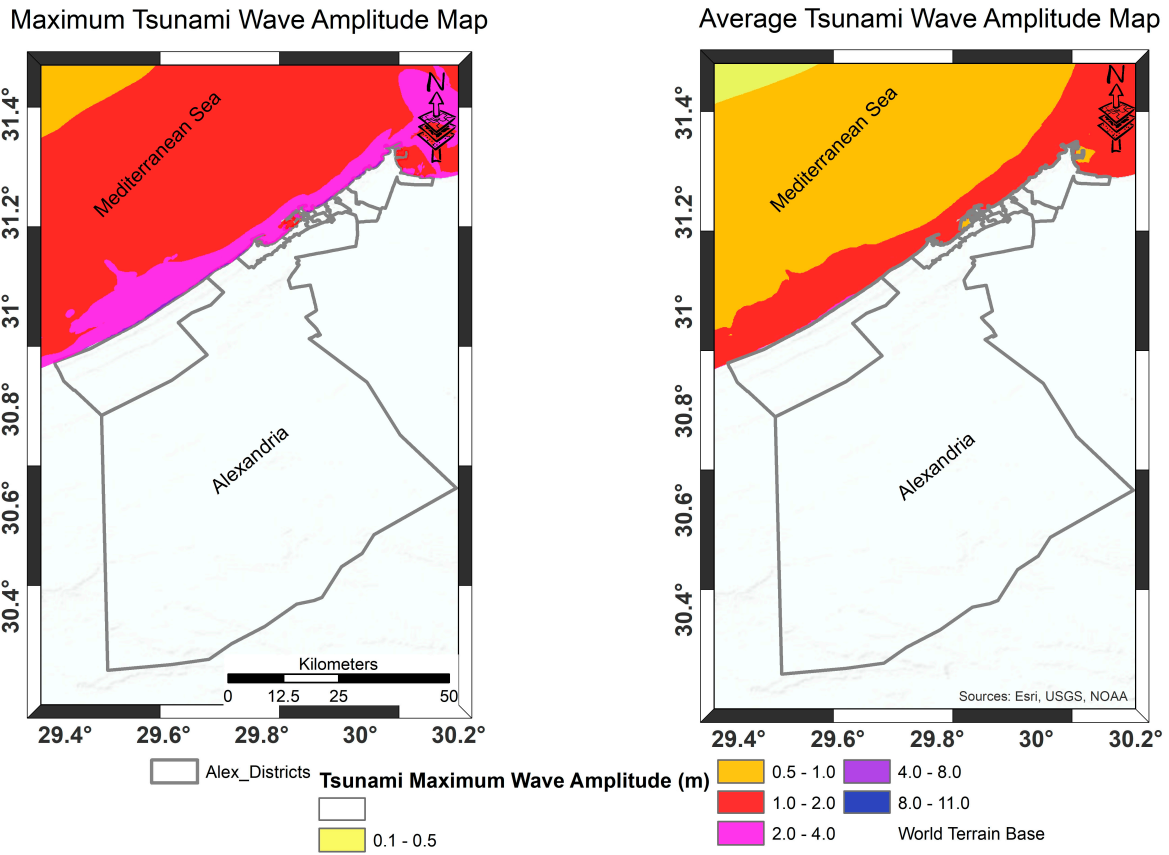
Maximum Tsunami Wave Amplitude Map

Average Tsunami Wave Amplitude Map

Figure 12. The aggregated scenario for Alexandria built from an envelope of the maximum and mean values of the tsunami wave amplitude produced by all individual scenarios listed in Table 3.
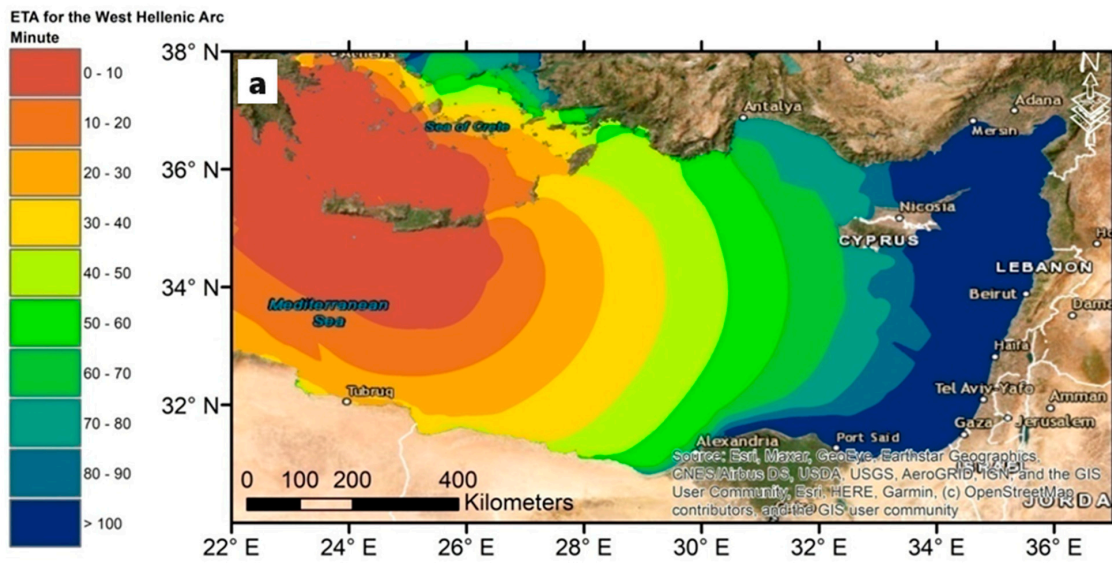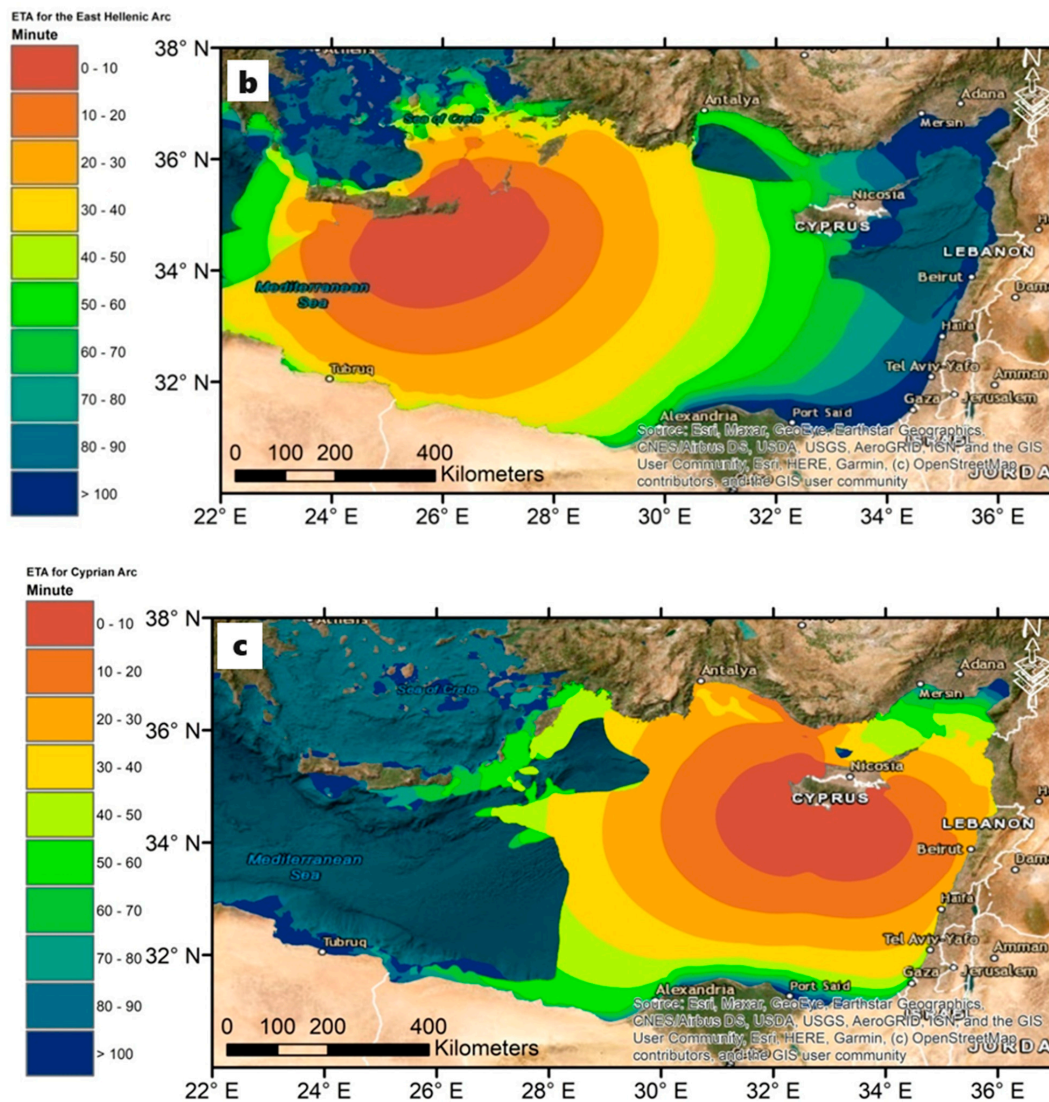

Figure 13. *Cont.*

Figure 13. The average ETA for representative scenarios in the East (**a**) and West Hellenic (**b**) and Cyprian (**c**) Arcs.

The maps of the mean and maximum tsunami wave amplitude were adopted to establish related tsunami inundation maps using various Coefficients and empirical relationships. In this work, we decided to take tsunami intensity as a representative value of the mean and maximum wave amplitude for the segmented shoreline, and each segment has a maximum tsunami wave amplitude value from the selected—then aggregated—tsunami scenarios developed by Hassan et al. [3]. To keep potential local changes in wave amplitude under consideration, which can lead to locally significant exceedance mediated on the coastal area, the tsunami amplitude must be applied to a multiplying safety factor, indicated with k. This coefficient allows for the transformation of the tsunami wave amplitude in an estimate of the maximum expected run-up, here indicated as R_{max}. To allow for a reliable choice of k, Basili et al. [71] produced an estimate of the relationship between tsunami amplitude and the maximum run-up R_{max} in some representative areas through the detailed modeling of numerous tsunamis with different features.

The simplest way to define the flooded area or inundation zone is to apply a hydrostatic model, based on a set scenario run-up value, without taking into account the resistance to the ingress of the tsunami wave on land, opposed by the roughness of the ground, both natural and artificial. In this case, the flooded area is the entire coastal strip located at a level lower than the run-up. This approach is very quick and easy to implement,

but, not considering the process of attenuation of the wave height inland, it can lead to a strong overestimation of the extension of the inundated areas. Therefore, it can be used for preliminary analyses on large areas and/or as a basis for orienting the choices of subsequent, more detailed processing. In this work, the inundation maps were developed by empirically taking into account the process of dissipation of the wave energy in its path on land. In practice, the method is based on the application of an empirical relationship between the scenario run-up and land penetration (Equation (1)), estimated on the basis of numerous observations conducted following recent and historical tsunami events, especially in the Pacific area (2004, 2011), but also in the Mediterranean. The use of GIS tools allows for the combination of topographic models of coastal areas with the empirical relationship of the attenuation of wave ingression, delimiting the inundated areas by classes of maximum potential scenario run-up values at the coast (Figure 3).

$$D = R/tg\alpha \tag{1}$$

where D is the inundation distance, R is the run-up, and $tg\alpha$ is the roughness; in this work, it varies between 0.015 and 0.08.

High inundation depth and zone are shown on the eastern side of the study area, as indicated in Figure 14. This highly inundated area occurs in the Al Montazah district, one of the busiest tourist districts during the summer. Also, the area around Alexandria Port, the middle of the study area, shows a large extent inundated area. This part of the city is highly commercial, social, and strategic, of great importance since this port is considered the largest in Egypt. However, the area located to the east of Alexandria, which imposes the highest tsunami hazard (Figure 14), has a high topography relative to the east side. Still, if no mitigation measures are applied, the existing water canals may augment or exaggerate the inundated area for the lowlands behind. The west of Alexandria, called Al Sahel Al Shamally, shows a less inundated area than the eastern side because it is naturally protected by a ridge of carbonate material that forms the shoreline. The west side of Alexandria's coast is less hazardous due to the presence of the ridge. The area between the shoreline and the road running along Alexandria's coast can be considered a highly hazardous zone for the people resting, swimming, and vacationing along the coast.
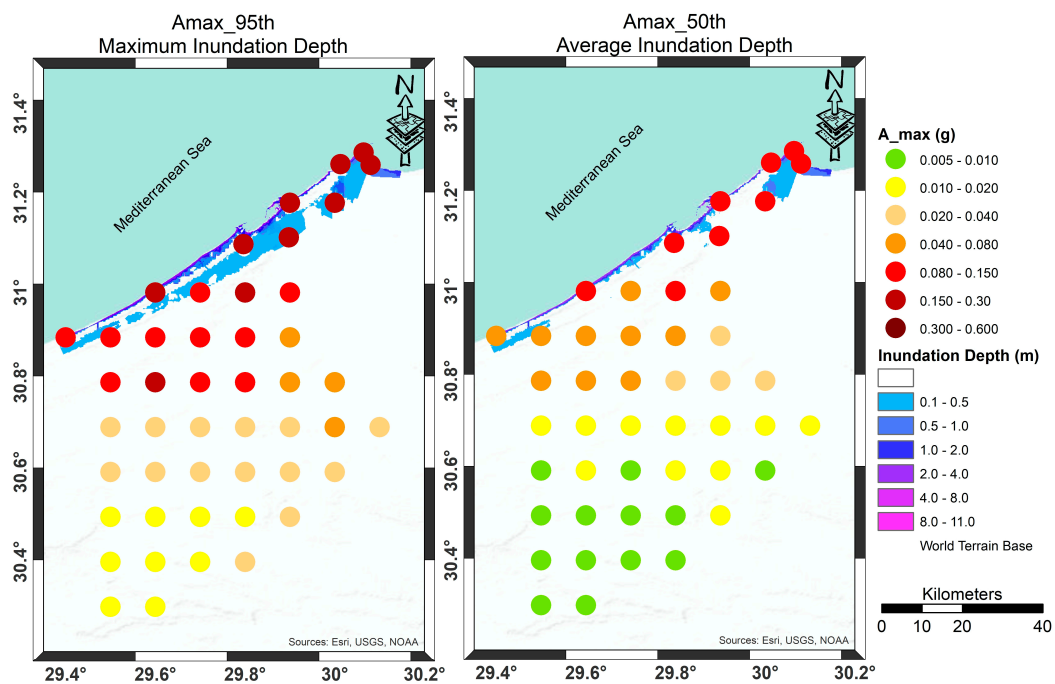

Figure 14. Joint peak ground acceleration (g) and inundation depth (m) (95th and 50th percentile) for the studied area.

5. Discussion and Conclusions

In our study, we utilized the NDSHA approach to investigate the seismic hazard in Alexandria on an urban scale. Our analysis included available information on seismogenic zones, levels of seismicity, and lithospheric geophysical properties, enabling us to compute physics-based synthetic seismograms and map them for observation sites across the study area. This study applied up-to-date seismogenic zones and earthquake catalogs (magnitude of 5.0 and more significant for the period 320–2020) for ground motion computations. The seismic engineering parameters (e.g., PGD, PGV, PGA, and spectral accelerations) that could be used to express the level of seismic hazard in a specific area can be easily extracted from these synthetic seismograms. Our study reveals that the northeastern region of Alexandria is characterized by moderate to high seismic hazards, particularly from sources originating in the Mediterranean Sea. The maximum ground acceleration in this area is estimated to be 0.15 g. By contrast, other parts of the city exhibit relatively lower seismic hazards.

Previous studies, including Ezzelarab et al. [12], reported maximum spectral acceleration (Sa) values of 0.03 g, 0.10 g, and 0.25 g for the spectral period of 0.1 s and return periods of 72, 475, and 2475 years, respectively, in Alexandria. Additionally, Sawires et al. [7] provided peak ground acceleration (PGA), Sa (0.1 s), and Sa (0.2 s) values of 0.09 g, 0.23 g, and 0.20 g, respectively, for a return period of 475 years. Seismic risk analysis for Alexandria was conducted by Badawy et al. [11], who estimated the percentage of expected damage to constructions to be around 2.2%, with 19% injuries and 0.01% fatalities. The study also identified the Al Montazah, Al Amereya, and Bab Sharq districts as having the highest seismic risk compared to other districts in Alexandria.

We also conducted a comprehensive tsunami inundation assessment for the Alexandria coastline by employing empirical relations based on average and maximum tsunami wave amplitude values for nine potential tsunamigenic earthquake scenarios taken from work by Hassan et al. [3]. We integrated information on the tsunami wave amplitude obtained for individual scenarios to create an aggregated scenario representing the maximum and mean expected wave amplitudes. An average ETA for the Hellenic and Cyprus Arc sources was also mapped, and its value for a tsunami in Alexandria falls within the range of 75–80 min. The aggregated inundation map shows that the districts of Al Gomrok and Al Montazah are the most vulnerable areas in Alexandria in the event of a tsunami. The western part of the city, known as Al Sahel Al Shamally, is less vulnerable to the impacts of a tsunami than the eastern side due to natural protection afforded by a ridge of carbonate material that runs parallel to the shoreline. However, it is essential to note that the water canals in this area could still contribute to the cascading of hazards.

Alexandria's susceptibility to local and regional earthquakes, which could trigger tsunamis and cause geological hazards on both land and sea, can have catastrophic economic and social consequences if each risk is addressed independently without considering their combined impact. It is crucial to study these hazards comprehensively and on an integrative basis. Also, visualization of multiple hazard assessment parameters is critical for developing effective and practical emergency response plans, enhancing public awareness, and implementing protective measures.

In this sense, Figure 14 displays an example of joint earthquake and tsunami hazard maps that can be valuable in the future if combined with high-resolution exposure and vulnerability models for multi-risk assessments for Alexandria. The joint earthquake and tsunami inundation maps, created using a GIS, show the peak ground acceleration and inundation depth resulting from various earthquake and tsunami scenarios at specific locations. The peak ground motion acceleration was calculated at selected observation sites and is represented by circles with color ranges corresponding to the values in g. Additionally, a tsunami inundation map for the coastal area is presented as a raster map with 30 × 30 m pixels, colored to reflect the inundation depth at each location in meters.

The results provided herein of tsunami hazard (inundation depth) estimations can play a significant role in the calibration and improvement of early warning systems for Egypt's coastal communities. The integration of tsunami wave amplitude and inundation depth

estimations into early warning systems can contribute to tsunami preparedness in Egypt generally, and in Alexandria specifically, by facilitating the establishment of evacuation routes and high-risk zones. This strengthens the ability of authorities to issue timely and targeted warnings, enhancing the safety and resilience of coastal communities in the face of tsunami threats. For urban planning purposes in Alexandria, we recommend that new projects be located in the southwestern part of the city. In fact, this area is characterized by a lower seismic and tsunami hazard risk compared to other parts of the city, making it a safer location for urban development.

The findings of this work provide critical insights into the risk reduction and disaster management system in Alexandria. The available exposure layers and vulnerability of the exposed asset can be used to estimate multi-risks for Alexandria. Moreover, the hazard assessment data can be integrated into real-time early warning systems that can significantly improve the timeliness and effectiveness of disaster responses. The results of this work can also be used in the updating of building codes and retrofitting guidelines to enhance the resilience of critical infrastructure. Urban planning strategies should leverage hazard maps to restrict development in high-risk areas and design safe evacuation routes.

References

1. Eckert, S.; Jelinek, R.; Zeug, G.; Krausmann, E. Remote sensing-based assessment of tsunami vulnerability and risk in Alexandria, Egypt. *Appl. Geogr.* **2012**, *32*, 714–723. [CrossRef]
2. Hassan, H.M.; Frischknecht, C.; ElGabry, M.N.; Hussein, H.; ElWazir, M. Tsunami hazard and risk assessment for Alexandria (Egypt) based on the maximum credible earthquake. *J. Afr. Earth Sci.* **2020**, *162*, 103735. [CrossRef]
3. Hassan, H.M.; Peresan, A.; ElGabry, M.N.; Hussein, H. Deterministic tsunamigenic earthquake hazard assessment for the northern coast of Egypt based on multi-scenario approach. *Mediterr. Geosci. Rev.* **2023**, *5*, 15–34. [CrossRef]
4. El-Sayed, A.; Wahlström, R. Distribution of the energy release, b-values and seismic hazard in Egypt. *Nat. Hazards* **1996**, *13*, 133–150. [CrossRef]
5. Badawy, A. Historical seismicity of Egypt. *Acta Geod. Geophys. Hung.* **1999**, *34*, 119–135. [CrossRef]
6. El-Sayed, A.; Vaccari, F.; Panza, G.F. Deterministic seismic hazard in Egypt. *Geophys. J. Int.* **2001**, *144*, 555–567. [CrossRef]
7. Sawires, R.; Peláez, J.A.; Fat-Helbary, R.E.; Ibrahim, H.A. An earthquake catalogue (2200 B.C. to 2013) for seismotectonic and seismic hazard assessment studies in Egypt. In *Earthquakes and Their Impact on Society*; D'Amico, S., Ed.; Springer: Cham, Switzerland, 2016; pp. 97–136. [CrossRef]
8. Hassan, H.M.; Romanelli, F.; Panza, G.F.; ElGabry, M.N.; Magrin, A. Update and sensitivity analysis of the neo-deterministic seismic hazard assessment for Egypt. *Eng. Geol.* **2017**, *218*, 77–89. [CrossRef]

9. Kamhawy, A.M.; Hassan, H.M.; ElKosery, H.M. Reappraisal of tsunami hazard for the Northern Coastal of Egypt considering sea level rise and delta subsidence scenarios. *Arab. J. Geosci.* **2023**, *16*, 220. [CrossRef]
10. El-Sayed, A.; Korrat, I.; Hussein, H.M. Seismicity and seismic hazard in Alexandria (Egypt) and its surroundings. *Seism. Ground Motion Large Urban Areas* **2004**, *161*, 1003–1019.
11. Badawy, A.; Gaber, H.; Ibrahim, H. Earthquake risk assessment of Alexandria, Egypt. *J. Seismol.* **2015**, *19*, 159–170. [CrossRef]
12. Ezzelarab, M.; Shokry, M.M.F.; Mohamed, A.M.E.; Helal, A.M.A.; Mohamed, A.A.; El-Hadidy, M.S. Evaluation of seismic hazard at the northwestern part of Egypt. *J. Afr. Earth Sci.* **2016**, *113*, 114–125. [CrossRef]
13. Ambraseys, N.N.; Melville, C.P.; Adams, R.D. *The Seismicity of Egypt, Arabia and the Red Sea*; Cambridge University Press: Cambridge, UK, 1995; p. 201. ISBN 0521391202.
14. Shah-Hosseini, M.; Saleem, A.; Mahmoud, A.M.A.; Morhange, C. Coastal boulder deposits attesting to large wave impacts on the Mediterranean coast of Egypt. *Nat. Hazards* **2016**, *83*, 849–865. [CrossRef]
15. Available online: https://qgis.org (accessed on 1 December 2024).
16. Central Agency for Public Mobilization and Statistics (CAPMAS). *Census of Population, Housing and Establishments, Internal Report*; CAPMAS: Cairo, Egypt, 2017.
17. Korrat, I.M.; El Agami, N.L.; Hussein, H.M.; El-Gabry, M.N. Seismotectonics of the passive continental margin of Egypt. *J. Afr. Earth Sci.* **2005**, *41*, 145–150. [CrossRef]
18. Abu El-Nader, I.F.; El Gabry, M.N.; Hussein, H.M.; Hassan, H.M.; Elshrkawy, A. Source characteristics of the Egyptian Continental margin earthquake, 19 October 2012. *Seismol. Res. Lett.* **2013**, *84*, 1062–1065. [CrossRef]
19. Badreldin, H.; Abdel-aal, A.K.; Toni, M.; El-Faragawy, K. Moment tensor inversion of small-to-moderate size local earthquakes in Egypt. *J. Afr. Earth Sci.* **2019**, *151*, 153–172. [CrossRef]
20. Rashwan, M.; Sawires, R.; Radwan, A.M.; Sparacino, F.; Peláez, J.A.; Palano, M. Crustal strain and stress fields in Egypt from geodetic and seismological data. *Remote Sens.* **2021**, *13*, 1398. [CrossRef]
21. Toni, M.; Badreldin, H.; El Fellah, Y. Seismicity and Seismotectonic of North Africa: An Updated Review. In *The Geology of North Africa. Regional Geology Reviews*; Hamimi, Z., Chabou, M.C., Errami, E., Fowler, A.-R., Fello, N., Masrouhi, A., Leprêtre, R., Eds.; Springer: Cham, Switzerland, 2024. [CrossRef]
22. Abdel-Aal, A.; Price, J.; Vaitl, D.J.; Shrallow, A. Tectonic evolution of the Nile Delta, its impact on sedimentation and hydrocarbon. In Proceedings of the 12th Petroleum Exploration and Production Conference, Cairo, Egypt, 12–15 November 1994; pp. 19–34.
23. Ahmed, A.A.; El Barkooky, A.; Gerrits, M.; Meyer, H.; Schwander, M.; Zaki, H. Tectonic evolution of the Eastern Mediterranean Basin and its significance for hydrocarbon prospectively in the ultra-deep water of the Nile Delta. *Lead. Edge* **2000**, *19*, 1086–1102.
24. Hussein, I.M.; Abd-Allah, A.M.A. Tectonic evolution of the northeastern part of the African continental margin, Egypt. *J. Afr. Earth Sci.* **2001**, *33*, 49–68. [CrossRef]
25. Mahmoud, S.; Reilinger, R.; McClusky, S.; Vernant, P.; Tealeb, A. GPS evidence for northward motion of the Sinai Block: Implications for, E. Mediterranean tectonics. *Earth Planet. Sci. Lett.* **2005**, *238*, 217–224. [CrossRef]
26. Reilinger, R.; McClusky, S.; Vernant, P.; Lawrence, S.; Ergintav, S.; Cakmak, R.; Ozener, H.; Kadirov, F.; Guliev, I.; Stepanyan, R.; et al. GPS constraints on continental deformation in the Africa-Arabia-Eurasia continental collision zone and implications for the dynamics of plate interactions. *J. Geophys. Res. Solid Earth* **2006**, *111*, B05411. [CrossRef]
27. Saleh, M.; Becker, M. New constraints on the Nubia–Sinai–Dead Sea fault crustal motion. *Tectonophysics* **2015**, *651*, 79–98. [CrossRef]
28. Kebeasy, R.M.; Maamoun, M.; Albert, R.N.H.; Megahed, M. Earthquake activity and earthquake risk around Alexandria, Egypt. *Bull. Int. Inst. Seismol. Earthq. Eng.* **1981**, *19*, 93–113.
29. El-Sayed, A.; Romanelli, F.; Panza, G. Recent seismicity and realistic waveforms modeling to reduce the ambiguities about the 1303 seismic activity in Egypt. *Tectonophysics* **2000**, *328*, 341–357. [CrossRef]
30. Guidoboni, E.; Ferrari, G.; Mariotti, D.; Comastri, A.; Tarabusi, G.; Valensise, G. Catalogue of Strong Earthquakes in Italy (461 BC-1997) and Mediterranean Area (760 BC-1500). 2007. Available online: https://www.earth-prints.org/entities/product/6258902c-f4ee-4938-9315-5cdc49ef2ffc/details-webproduct (accessed on 1 December 2024).
31. Ali, S.M.; Badreldin, H. Present-day stress field in Egypt based on a comprehensive and updated earthquake focal mechanisms catalog. *Pure Appl. Geophys.* **2019**, *176*, 4729–4760. [CrossRef]
32. Ambraseys, N. *Earthquakes in the Mediterranean and Middle East: A Multidisciplinary Study of Seismicity up to 1900*; Cambridge University Press: Cambridge, UK, 2009.
33. Maamoun, M.; Allam, A.; Megahed, A. Seismicity of Egypt. *Bull. HIAG* **1984**, *4*, 109–160.
34. Hassoup, A.; Tealab, A. Attenuation of intensity in the northern part of Egypt associated with the May 28, 1998 Mediterranean. *Acta Geophys. Pol.* **2000**, *38*, 183–196.
35. Guidoboni, E.; Comastri, A. The large earthquake of 8 August 1303 in Crete: Seismic scenario and tsunami in the Mediterranean area. *J. Seismol.* **1997**, *1*, 55–72. [CrossRef]
36. Meghraoui, M. Paleoseismic history of the Dead Sea fault zone. *Encycl. Earthq. Eng.* **2015**. [CrossRef]
37. NRIAG. Historical seismicity of Egypt. In *A Study for Previous Catalogues Producing Revised Weighted Catalogue, Proceedings of the Second Arab Conference for Astronomy and Geophysics, Cairo, Egypt, 25–28 October 2010*; Springer Science and Business Media LLC: New York, NY, USA, 2010.

38. NRIAG Earthquake Annual Bulletins 2021. Issued Under the Authority of the Egyptian National Seismic Network-ENSN, Seismology Department, National Research Institute of Astronomy and Geophysics. Available online: https://www.nriag.sci.eg/wp-content/uploads/2023/03/Earthquakes-Annual-Bulletin-2021.pdf (accessed on 1 January 2021).

39. Reiter, L. *Earthquake Hazard Analysis: Issues and Insights*; Columbia University Press: New York, NY, USA, 1991.

40. Kramer, S.L.; Stewart, J.P. *Geotechnical Earthquake Engineering*; CRC Press: Boca Raton, FL, USA, 2024.

41. Bela, J.; Panza, G.F. Ndsha-the new paradigm for rsha-an updated review. *Vietnam. J. Earth Sci.* **2021**, *43*, 111–188. [CrossRef] [PubMed]

42. Bela, J.; Kossobokov, V.; Panza, G. Seismic Rigoletto: Hazards, risks and seismic roulette applications. *Front. Earth Sci.* **2023**, *11*, 1136472. [CrossRef]

43. Panza, G.F.; Bela, J. NDSHA: A new paradigm for reliable seismic hazard assessment. *Eng. Geol.* **2020**, *275*, 105403. [CrossRef]

44. Panza, G.F.; Romanelli, F.; Vaccari, F. Seismic wave propagation in laterally heterogeneous anelastic media: Theory and applications to seismic zonation. In *Advances in Geophysics*; Elsevier: Amsterdam, The Netherlands, 2001; Volume 43, pp. 1–95.

45. Panza, G.; Kossobokov, V.G.; Laor, E.; DeVivo, B. *Earthquakes and Sustainable Infrastructure: Neodeterministic (NDSHA) Approach Guarantees Prevention Rather Than Cure*; Elsevier: Amsterdam, The Netherlands, 2021.

46. Mourabit, T.; Elenean, K.A.; Ayadi, A.; Benouar, D.; Suleman, A.B.; Bezzeghoud, M.; Cheddadi, A.; Chourak, M.; ElGabry, M.N.; Harbi, A.; et al. Neo-deterministic seismic hazard assessment in North Africa. *J. Seismol.* **2014**, *18*, 301–318. [CrossRef]

47. Magrin, A.; Parvez, I.A.; Vaccari, F.; Peresan, A.; Rastogi, B.K.; Cozzini, S.; Bisignano, D.; Romanelli, F.; Choudhury, P.; Roy, K.S.; et al. Neo-deterministic definition of seismic and tsunami hazard scenarios for the territory of Gujarat (India). In *Earthquakes and Their Impact on Society*; Springer: Cham, Switzerland, 2016; pp. 193–212.

48. Romanelli, F.; Vaccari, F.; Cantagallo, C.; Camata, G.; Panza, G.F. Physics-Based Approach to Define Energy-Based Seismic Input: Application to Selected Sites in Central Italy. In *International Workshop on Energy-Based Seismic Engineering*; Springer: Cham, Switzerland, 2023; pp. 112–128.

49. Aki, K. A perspective on the history of strong motion seismology. *Phys. Earth Planet. Inter.* **2003**, *137*, 5–11. [CrossRef]

50. Hussein, H.M.; Abou Elenean, K.M.; Marzouk, I.A.; Peresan, A.; Korrat, I.M.; Abu El-Nader, E.; Panza, G.F.; El-Gabry, M.N. Integration and magnitude homogenization of the Egyptian earthquake catalogue. *Nat. Hazards* **2008**, *47*, 525–546. [CrossRef]

51. Rugarli, P.; Amadio, C.; Peresan, A.; Fasan, M.; Vaccari, F.; Magrin, A.; Romanelli, F.; Panza, G.F. Neo-Deterministic Scenario-Earthquake Accelerograms and Spectra: A NDSHA Approach to Seismic Analysis. In *Structural Engineering in Vibrations, Dynamics and Impacts*; Jia, J., Paik, J.K., Eds.; CRC Press, Taylor & Francis Group: Abingdon, UK, 2019.

52. Joint Research Centre (European Commission); Aucun, B.; Fajfar, P.; Franchin, P.; Carvalho, E.; Kreslin, M.; Pecker, A.; Tsionis, G.; Pinto, P.; Degee, H.; et al. *Eurocode 8—Seismic Design of Buildings—Worked Examples*; Aucun, B., Carvalho, E., Pinto, P., Fardis, M., Eds.; Publications Office: Luxembourg, 2012; Available online: https://data.europa.eu/doi/10.2788/91658 (accessed on 1 December 2024).

53. Jelínek, R.; Eckert, S.; Zeug, G.; Krausmann, E. Tsunami vulnerability and risk analysis applied to the city of Alexandria, Egypt. In *Tsunami Risk and Strategies for the European Region (TRANSFER)*; Office for Official Publications of the European Communities: Luxembourg, 2009.

54. TSUMAPS-NEAM-2018. Available online: https://www.tsumaps-neam.eu/ (accessed on 1 January 2023).

55. Pagnoni, G.; Armigliato, A.; Tinti, S. Scenario-based assessment of buildings damage and population exposure due to tsunamis for the town of Alexandria, Egypt. *Nat. Hazards Earth Syst. Sci. Discuss.* **2015**, *3*, 5085–5154. [CrossRef]

56. Dogan, G.G.; Yalciner, A.C.; Yuksel, Y.; Ulutaş, E.; Polat, O.; Güler, I.; Şahin, C.; Tarih, A.; Kânoğlu, U. The 30 October 2020 Aegean Sea tsunami: Post-event field survey along Turkish coast. *Pure Appl. Geophys.* **2021**, *178*, 785–812. [CrossRef] [PubMed]

57. Heidarzadeh, M.; Necmioglu, O.; Ishibe, T.; Yalciner, A.C. Bodrum–Kos (Turkey–Greece) Mw 6.6 earthquake and tsunami of 20 July 2017: A test for the Mediterranean tsunami warning system. *Geosci. Lett.* **2017**, *4*, 31. [CrossRef]

58. DeMets, C.; Gordon, R.G.; Argus, D.F.; Stein, S. Current plate motions. *Geophys. J. Int.* **1990**, *101*, 425–478. [CrossRef]

59. McClusky, S.; Balassanian, S.; Barka, A.; Demir, C.; Ergintav, S.; Georgiev, I.; Gurkan, O.; Hamburger, M.; Hurst, K.; Kahle, H.; et al. Global Positioning System constraints on plate kinematics and dynamics in the eastern Mediterranean and Caucasus. *J. Geophys. Res. Solid Earth* **2000**, *105*, 5695–5719. [CrossRef]

60. Tinti, S.; Armigliato, A.; Pagnoni, G.; Zaniboni, F. Scenarios of giant tsunamis of tectonic origin in the Mediterranean. *ISET J. Earthq. Technol.* **2005**, *42*, 171–188.

61. Papadopoulos, G.A.; Daskalaki, E.; Fokaefs, A.; Giraleas, N. Tsunami hazards in the Eastern Mediterranean: Strong earthquakes and tsunamis in the East Hellenic Arc and Trench system. *Nat. Hazards Earth Syst. Sci.* **2007**, *7*, 57–64. [CrossRef]

62. Ambraseys, N.; Synolakis, C. Tsunami catalogs for the Eastern Mediterranean, revisited. *J. Earthq. Eng.* **2010**, *14*, 309–330. [CrossRef]

63. Galanopoulos, A.G. Tsunamis observed on the coasts of Greece from antiquity to present time. *Ann. Geophys.* **1960**, *13*, 369–386. [CrossRef]

64. Papadopoulos, G.A.; Chalkis, B.J. Tsunamis observed in Greece and the surrounding area from antiquity up to the present times. *Mar. Geol.* **1984**, *56*, 309–317. [CrossRef]

65. Papazachos, B.C.; Koutitas, C.; Hatzidimitriou, P.M.; Karacostas, B.G.; Papaioannou, C.A. Tsunami hazard in Greece and the surrounding area. *Ann. Geophys.* **1986**, *4*, 79–90.

66. Papazachos, B.C.; Dimitriu, P.P. Tsunamis in and near Greece and their relation to the earthquake focal mechanisms. In *Tsunami Hazard*; Springer: Dordrecht, The Netherlands, 1991; pp. 161–170.

67. DISS Working Group. *Database of Individual Seismogenic Sources (DISS)*, Version 3.2; Istituto Nazionale di Geofisica e Vulcanologia (INGV): Rome, Italy, 2020.

68. DISS Working Group. *Database of Individual Seismogenic Sources (DISS)*, Version 3.3; Istituto Nazionale di Geofisica e Vulcanologia (INGV): Rome, Italy, 2021.

69. Bilham, R. Tsunamigenic middle earth. *Nat. Geosci.* **2008**, *1*, 211–212. [CrossRef]

70. England, P.; Howell, A.; Jackson, J.; Synolakis, C. Palaeotsunamis and tsunami hazards in the Eastern Mediterranean. *Philos. Trans. R. Soc. A Math. Phys. Eng. Sci.* **2015**, *373*, 20140374. [CrossRef]

71. Basili, R.; Brizuela, B.; Herrero, A.; Iqbal, S.; Lorito, S.; Maesano, F.E.; Murphy, S.; Perfetti, P.; Romano, F.; Scala, A.; et al. The making of the NEAM tsunami hazard model 2018 (NEAMTHM18). *Front. Earth Sci.* **2021**, *8*, 616594. [CrossRef]